

THESIS FOR THE DEGREE OF LICENTIATE OF PHILOSOPHY

On hydrogen point defects in perovskite oxides

ERIK JEDVIK GRANHED

*Department of Physics*

CHALMERS UNIVERSITY OF TECHNOLOGY

Göteborg, Sweden 2017

On hydrogen point defects in perovskite oxides  
ERIK JEDVIK GRANHED

© Erik Jedvik Granhed, 2017

Department of Physics  
Chalmers University of Technology  
SE-412 96 Göteborg, Sweden  
Telephone +46 31 772 10 00

Chalmers reproservice  
Göteborg, Sweden 2017

# On hydrogen point defects in perovskite oxides

ERIK JEDVIK GRANHED

*Department of Physics*

Chalmers University of Technology

---

## Abstract

Oxides based on the perovskite structure exhibit a surprisingly large diversity in materials properties and are found in many different applications, several related to clean energy technologies, such as solar cells, batteries and fuel cells. Many properties in materials are the result of lattice imperfections, commonly denoted *defects*, and much effort is devoted to fine tuning materials properties through controlling the defects therein. Therefore, a thorough understanding of defect properties on a microscopic scale is desirable, and first-principles calculations have proven an invaluable tool in complementing experimental observations. In the present thesis density functional theory (DFT) calculations have been employed to describe two types of hydrogen point defects in perovskite oxides with the aim of deepening the understanding as well as to develop tools for modelling and characterising point defects. In paper I a strain tensor formalism for describing the anisotropic volume expansion of a point defect is developed. The formalism is successfully applied to the proton forming a hydroxide ion and the oxygen vacancy in acceptor-doped barium zirconate. It is inferred that both the hydroxide ion and the oxygen vacancy are smaller than the oxygen host ion, but that the difference in size causes an expansion in hydration which could lead to micro-cracking of the material. In paper II the substitutional hydride ion on an oxygen site in barium titanate is investigated. For this oxyhydride material two possible electronic states are permissible leading to different conductive properties; on the one hand the delocalised band-state as predicted by band theory and on the other hand a polaron state, in which an electron localises on one of the titanium ions next to the hydride ion, the description of which requires beyond DFT-methods. The two electronic states are investigated through their influence on the hydrogen vibrations, using both theoretical methods and inelastic neutron scattering measurements, and through their different volume expansion. The conclusion that the electronic state is predominantly band-like is confirmed both through the vibrational characterisation and the strain tensor formalism. The thesis reiterates the usefulness of first-principles calculations in assisting interpretation of experimental data.

**Keywords:** BaZrO<sub>3</sub>, BaTiO<sub>3</sub>, point defects, proton conductor, chemical expansion, oxyhydride, polaron, phonon, density functional theory



## LIST OF PUBLICATIONS

This thesis consists of an introductory text and the following papers:

**I Size and shape of oxygen vacancies and protons in acceptor-doped barium zirconate**

Erik Jedvik, Anders Lindman, Magnús Þór Benediktsson and Göran Wahnström  
Solid State Ionics 275 (2015) 2-8

**II Vibrational characterization of electronic defects in oxyhydride barium titanate**

Erik Jedvik Granhed, Anders Lindman, Carin Österberg, Maths Karlsson and Göran Wahnström  
To be Submitted

Specification of the authors contribution to the publications:

- I The author performed the theoretical modelling, all DFT calculations and wrote the first draft of the paper.
- II The author performed all DFT and phonon calculations and co-authored the paper. The analysis was performed jointly.



# Contents

<b>1</b>	<b>Introduction</b>	<b>1</b>
<b>2</b>	<b>The perovskite structure</b>	<b>3</b>
2.1	Ideal crystal structure . . . . .	3
2.2	Distorted crystal structures . . . . .	4
2.3	Tilts and instabilities . . . . .	5
2.4	Point defects . . . . .	6
2.5	Hydration . . . . .	8
2.6	The oxyhydride barium titanate . . . . .	9
2.7	Polaron as a quasi-particle . . . . .	10
<b>3</b>	<b>Energy of point defect formation</b>	<b>13</b>
3.1	Formation energy . . . . .	13
3.2	Chemical potentials for the gas phases . . . . .	14
3.3	Vibrational free energy for the solid phases . . . . .	15
3.3.1	Effect of constant pressure vs constant volume . . . . .	16
3.4	Configurational entropy . . . . .	17
<b>4</b>	<b>Chemical expansion</b>	<b>19</b>
4.1	A thermodynamics view on strain . . . . .	19
4.2	The defect induced strain tensor . . . . .	20
4.3	Strain in one dimension . . . . .	20
4.4	The strain tensor . . . . .	21
<b>5</b>	<b>Electronic structure calculations</b>	<b>25</b>
5.1	Adiabatic Approximation . . . . .	26
5.2	The Hartree-Fock approximation . . . . .	27
5.3	The Hohenberg-Kohn Theorems . . . . .	29
5.4	The Kohn-Sham Approach . . . . .	30
5.5	The Kohn-Sham equations . . . . .	30
5.6	Approximations to the Exchange-Correlation Functional . . . . .	31

5.6.1	Local Density Approximation . . . . .	31
5.6.2	Generalised Gradient Approximation . . . . .	32
5.6.3	Hybrid functionals . . . . .	32
5.6.4	DFT+ $U$ – “poor man’s hybrid” . . . . .	33
5.7	Implementation in periodic solids . . . . .	34
5.7.1	Plane waves . . . . .	34
5.7.2	Finite sampling . . . . .	35
5.7.3	Pseudopotentials and PAW . . . . .	36
<b>6</b>	<b>Vibrational motion</b>	<b>37</b>
6.1	One-dimensional diatomic chain . . . . .	37
6.1.1	High symmetry points . . . . .	39
6.1.2	Limiting cases I. Identical masses . . . . .	41
6.1.3	Limiting cases II. Localised vibrations . . . . .	41
6.1.4	Application in oxyhydrides . . . . .	41
6.2	Phonons as lattice modes . . . . .	42
6.2.1	$q$ -space . . . . .	43
6.2.2	Atomic displacements . . . . .	44
6.2.3	Bandspectrum . . . . .	45
6.2.4	Density of State . . . . .	45
6.2.5	Limiting case. Localised modes. . . . .	47
6.2.6	Lattice stability . . . . .	48
6.3	Computational aspects . . . . .	49
6.3.1	Localised hydrogen modes . . . . .	50
<b>7</b>	<b>Summary of appended articles</b>	<b>53</b>
7.1	Paper I . . . . .	53
7.2	Paper II . . . . .	54
<b>8</b>	<b>Summary and Outlook</b>	<b>55</b>
	<b>Acknowledgments</b>	<b>57</b>
	<b>Bibliography</b>	<b>59</b>
	<b>Papers I-II</b>	<b>69</b>

# Introduction

When we talk colloquially about defects the implication is often of a negative property or even detrimental flaw. And indeed, defects change the properties of the host material and can lead to unwanted effects if not properly controlled. However, when properly controlled, defects are the material engineer's way of tuning material properties into desired ditos. The semi-conductor industry, for example, relies heavily on such manipulation of the material through point-defects.

Defects come in such variety that the possibilities seem endless. While the number of elements in the periodic table is limited already the number of combinations containing two elements is large. The number of possible configurations by introducing just one point defect is even larger. In addition to which element is chosen, the defect can be placed in many different sites and be in different charge states, leading to different material properties. Therefore, a thorough understanding of point defects on a microscopic scale is crucial to the understanding of material properties.

Owing to its intrinsic zero dimensional nature, a point defect, or any single atom, is difficult to observe experimentally and much of the knowledge about point defects is inferred by implicit methods. The still relatively recent development of first principle methods, such as the density functional theory, has therefore proved an invaluable tool in modelling the microscopic origin of macroscopic phenomena.

Hydrogen as a point defect is found in many applications, e.g., in proton conducting ceramics such as the perovskite  $\text{BaZrO}_3$  [1]. In order to improve the proton conduction a thorough understanding of the diffusion mechanisms is important. However, in the pursuit of knowledge and understanding it is desirable to broaden the perspective also to other types of hydrogen defects which may lead to new insights and new perspectives.

The aim with the present thesis is to deepen the understanding of hydrogen

## Chapter 1. Introduction

---

point defects in perovskite oxides as well as to develop tools for modelling and characterising point defects.

# The perovskite structure

Perovskite is a mineral named after the Russian mineralogist Count Lev Perovski [2]. Perovskite has a very distinctive crystal structure and although the perovskite mineral is composed of calcium titanate ( $\text{CaTiO}_3$ ) its crystal structure is shared by many other compounds. Other materials exhibiting perovskite structure are often, although somewhat incorrectly, called perovskites. We will adopt this terminology of calling a material exhibiting the perovskite structure a *perovskite*.

Perovskites are rather extensively studied due to the abundance of properties exhibited by different perovskites in combination with their rather simple crystal structure. Bhalla *et al.* [3] even claim it is “the single most versatile ceramic host”. Among the properties exhibited by perovskites are high dielectric constant [4], ferro- and anti-ferro-electricity [5], piezoelectricity [6], magnetoresistance [7, 8], thermoelectricity [9], superconductivity [10, 11], oxygen ion conduction [12] and last but not least proton conductivity [1].

## 2.1 Ideal crystal structure

A perovskite is an  $\text{ABO}_3$  compound, where A and B are cations whose formal charge sum is +6 and the O is the  $-2$  charge anion.<sup>1</sup> This makes the perovskite as a whole charge balanced. Due to the limited restriction on the valency of the A and B atoms, the charge sum of +6 may be either 1+5, 2+4 or 3+3, there is an abundance of perovskites [2, 13]. Many more structures can also be constructed by alloying on the A or B site. The ‘ideal’ perovskite structure, shown in Figure 2.1a, is simple cubic with the A atoms in the corners (0,0,0), B atoms in the body centre

---

<sup>1</sup>Other species are possible in stead of oxygen, such as F, N or H. These can also be referred to as perovskites, but we will limit the discussion to oxides.

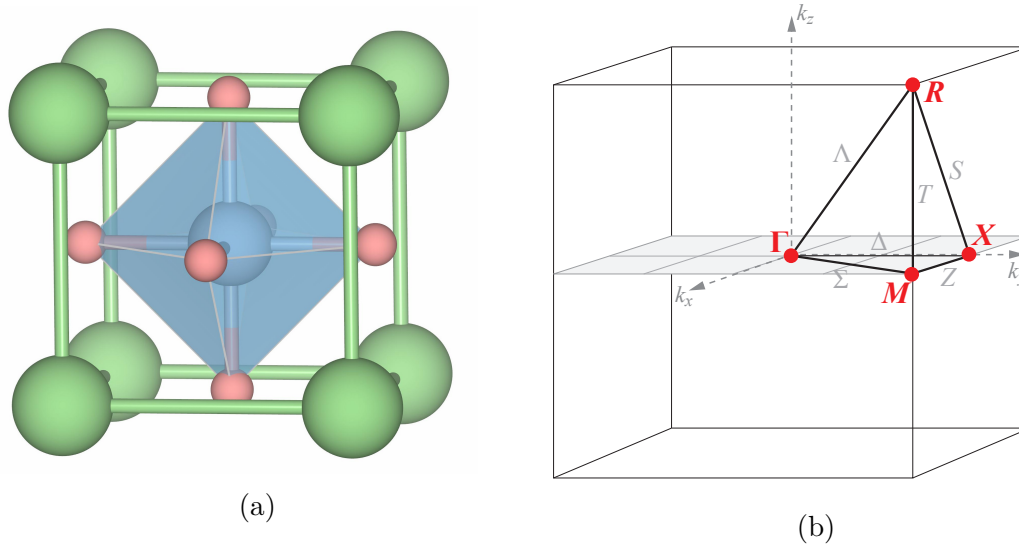


Figure 2.1: (a) The cubic crystal structure of the ideal perovskite with symmetry  $Pm\bar{3}m$  together with its octahedron dual. The A atoms are marked green, the B atoms blue and oxygen red. (b) The Brillouin zone of the cubic perovskite.

$(\frac{1}{2}, \frac{1}{2}, \frac{1}{2})$  and oxygen on the faces,  $(\frac{1}{2}, \frac{1}{2}, 0)$ . The A atoms are shared between eight unit cells to a total of one A-atom per unit cell. Similarly the oxygen atoms are shared between two cells which yields a total of 3 oxygen per unit cell.

A very important aspect of a crystal is its *reciprocal* cell. The reciprocal cell is the Fourier transform of the (primitive) unit cell of the real space crystal lattice. It is a convenient mathematical construction in which both electronic and vibrational properties of a crystal can be calculated and visualised. The reciprocal unit cell, also known as the Brillouin zone, of a simple cubic lattice, such as the perovskite structure, is also simple cubic and shown in Figure 2.1b. Due to the symmetries of the cube it is customary to specify the properties only at certain points, the high symmetry points, and along the lines connecting them. In Figure 2.1b the high symmetry points  $\Gamma$ ,  $X$ ,  $M$  and  $R$  corresponding to the points  $(0,0,0)$ ,  $(0,0,\frac{1}{2})$ ,  $(0,\frac{1}{2},\frac{1}{2})$  and  $(\frac{1}{2},\frac{1}{2},\frac{1}{2})$  are shown.

## 2.2 Distorted crystal structures

Very few perovskites exhibit the ideal cubic structure [2, 13]. In fact, not even  $\text{CaTiO}_3$ , the perovskite mineral itself, is truly cubic. Since most perovskites are considered to be ionic, the ions building up the crystal can to a first approximation be regarded as hard spheres with ionic radii  $R$ . For such a model, the lattice

constant as measured along the B-O-B axis equals  $a = 2R_A + 2R_O$  or if measured along the face diagonal  $\sqrt{2}a = 2R_B + 2R_O$ . Due to the differences in ionic radii in real materials these two measurements lead to different lattice constant, and the discrepancy is accommodated for in the *tolerance factor* or Goldschmidt ratio [14].

$$t = \frac{R_A + R_O}{\sqrt{2}(R_B + R_O)} \quad (2.1)$$

A tolerance factor close to unity is assumed to favour the ideal cubic perovskite structure.

With the ionic radii defined by Shannon [15] the tolerance factor is 1.002 for SrTiO<sub>3</sub>, which is indeed cubic at room temperature [16]. So is BaZrO<sub>3</sub>, which is studied in **Paper I**, with a tolerance factor of 1.004. A tolerance factor in the interval  $0.9 < t < 1$  often implies cubic structure [13] but a tolerance factor lower than unity will in general favour distortions into structures of lower symmetry. For example, although CaTiO<sub>3</sub> has a tolerance factor of 0.97, which is near unity, CaTiO<sub>3</sub> is orthorhombic at room temperature. Tolerance factors larger than unity also cause distortions, generally towards hexagonal close-packed structure [2]. BaTiO<sub>3</sub>, which is the material investigated in **Paper II**, has a tolerance factor of 1.06 and is not cubic at room temperature, but has a different kind of distortion into tetragonal symmetry and it is not until at a temperature of 120°C that BaTiO<sub>3</sub> becomes cubic.

Although the tolerance factor may serve as a first guide to the crystal structure of a perovskite it is but a rough estimate. Even SrTiO<sub>3</sub>, which is cubic at room temperature and has a tolerance factor close to 1 undergoes a phase transition when cooled.

## 2.3 Tilts and instabilities

A tilt consists of a rotation of the inscribed BO<sub>6</sub> octahedron about the pseudo-cubic axes. The octahedron, illustrated in Figure 2.1a, is regarded as rigid and a rotation leaves the B-atom centred in the cage, but does not disrupt its corner sharing connectivity.

The tilts can be designated according to Glazer [17,18] by the rotations along the three Cartesian coordinates axes, which coincide with the basis vectors. General, unequal, rotations about the axes  $x$ ,  $y$  and  $z$  are denoted by  $a$ ,  $b$  and  $c$  with a superscript  $+$  indicating tilts in successive layers in the same direction, i.e. in-phase rotation, and  $-$  in opposite directions, i.e. out-of-phase rotation. A zero superscript indicates no rotation. Thus a rotation  $a^+b^+c^+$  indicates three unequal rotations about the axes  $x$ ,  $y$  and  $z$ , with the octahedra along the axes tilted the same way. The  $R$ -point instability exhibited by SrTiO<sub>3</sub> (cf. Section 6.2.6) is a

$a^0a^0c^-$  tilt indicating a rotation about the  $z$ -axis with successive layers in opposite directions. This is illustrated in Figure 2.2b. In order to leave the oxygen octahedra rigid the lattice constants must change during a tilt, and for the rotation around the  $z$ -axis the lattice constant in the  $x$  and  $y$  direction decrease by an equal amount leading to a tetragonal  $I4/mcm$  symmetry.

The distortion in  $\text{BaTiO}_3$  differs from the octahedral tilting mentioned above insofar as that the A and B-cations are displaced relative to the polyhedral centres of coordination. This causes a permanent electric dipole moment, which is the cause of the ferroelectricity exhibited by  $\text{BaTiO}_3$ . There are three possible directions for the B-cation displacement; along the  $[100]$  direction, the  $[110]$  direction and the  $[111]$  direction. These displacements cause distortions into crystals of tetragonal, orthorhombic and rhombohedral symmetry, respectively.  $\text{BaTiO}_3$  is important because it exhibits all these three phases and is therefore sometimes considered as the prototypical ferroelectric [19]. The tilt exhibited by  $\text{SrTiO}_3$  also carries a local dipole moment which is out-of-phase from one unit cell to the next.  $\text{SrTiO}_3$  therefore exhibits anti-ferroelectricity.

It is important to understand tilts and structural phase transitions in perovskites. Calculations are generally performed at zero kelvin. If the investigated phase is stable only at elevated temperatures, such as the cubic phase of  $\text{BaTiO}_3$ , a slight perturbation of the stoichiometry might induce not only a point defect but also a structural phase transition. To be able to identify a structural phase transition and prevent or remove unwanted structural transitions in a defect calculation is crucial for obtaining correct formation energies.

## 2.4 Point defects

In addition to the structural instabilities discussed above, all real materials contain defects, including point defects such as vacancies and interstitials, line defects such as dislocations and plane defects such as grain boundaries. In this thesis the focus is on three types of point defects; interstitials, vacancies and substitutional defects. These are illustrated schematically in Figure 2.3. A point defect is a non-stoichiometric perturbation of the ideal lattice which may or may not be electrically charged. Point defects cause an increase of the configurational entropy contribution to the free energy at non-zero temperatures and will therefore always be present. Materials can also be prepared in such a way as to increase the number of defects. This is referred to as doping and is performed, e.g. to make  $\text{BaZrO}_3$  proton conducting.

By substituting a tetravalent zirconium ion with a trivalent ion, such as yttrium, a *substitutional* defect is created. In Kröger-Vink notation, which is often used in defect chemistry, this is written as  $Y'_{\text{Zr}}$ , where Y denotes yttrium and the subscript

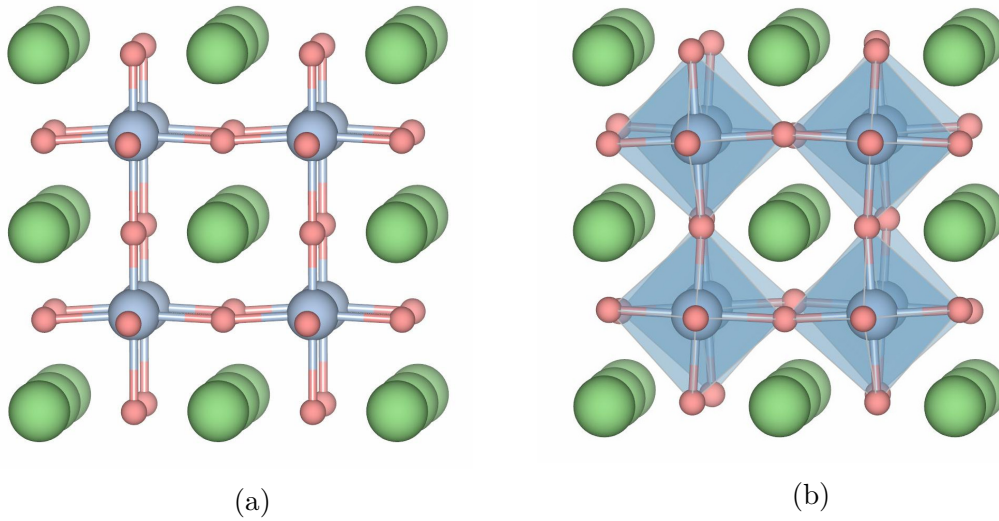


Figure 2.2: (a) The ferroelectric distortion of BaTiO<sub>3</sub> into the tetragonal  $P4mm$  and (b) the  $a^0a^0c^-$  anti-ferroelectric distortion of the SrTiO<sub>3</sub> into the tetragonal  $I4/mcm$  crystal structure.

Zr indicates the host site. While zirconium donates four electrons to the lattice making the zirconium ion charged +4, yttrium donates only three and the yttrium ion is charged +3. Since the defect charge is given relative to the original site in Kröger-Vink notation the apostrophe indicates a defect charge of  $-1$ .

A *vacancy* is formed by removal of an atom, e.g. an oxygen atom. Since the oxygen ion has a charged of  $-2$  the defect left behind after removal of an oxygen atom will be  $v_{\text{O}}^{\bullet\bullet}$  in Kröger-Vink notation, where  $v$  indicates a vacancy<sup>2</sup>, the subscript O indicates the oxygen host site and the defect charge of +2 is denoted by two dots. Thus the combination of e.g., two yttrium substitutional defects and one oxygen vacancy makes the material charge neutral. Alloying with substitutional defects in this manner is usually referred to as acceptor doping due to the similarities to semiconductor doping.

An *interstitial* is an ion situated between ideal lattice sites. An interstitial can be of any type, including those already found in the host, and is denoted by an index  $i$ . A proton ( $\text{H}^+$ ) interstitial would for example be denoted  $\text{H}_i^{\bullet}$ , where the dot denotes the positive charge of the proton. The proton studied in **Paper I** however, is so closely bound to the nearest neighbour oxygen that the notation  $(\text{OH})_{\text{O}}^{\bullet}$  is more appropriate.

<sup>2</sup>Vacancies are often denoted with an upper-case V. Here we adhere to the convention of using lower-case to avoid confusion with a substitutional vanadium. Similarly a lower-case  $i$  is used to denote the interstitial.

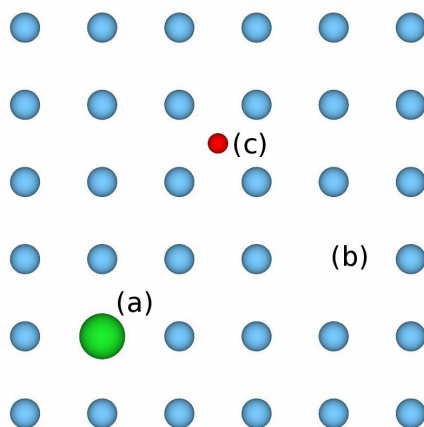


Figure 2.3: Schematic illustration of (a) a substitutional defect (b) a vacancy and (c) an interstitial.

It is often necessary to include a non-defect site in chemical reaction formulas. The notation for an ideal site is written  $O_O^\times$ , which is an oxygen on an oxygen site with neutral charge.

## 2.5 Hydration

In **Paper I** the hydration of a  $BaZrO_3$  is studied. Although a small number of vacancies can be present also in undoped  $BaZrO_3$  a higher concentration of vacancies is made possible by the presence of acceptor doping, such as yttrium in  $BaZrO_3$ . During hydration an oxygen vacancy is filled and two hydroxide ions are formed.



The hydrogen atom is rather loosely bound to the oxygen and is mobile in the shape of a positively charged proton, making the material proton conducting.

In analogy with the ionic radii of atoms, the vacancy is often described in terms of an ionic radius. This is intrinsically difficult and the modelling of a vacancy as a hard sphere is problematic as the vacancy should rather be modelled as the lack of one. Similarly, the proton can be given an ionic radius. Usually, the radius is not assigned to the proton itself, but to the hydroxide ion. The difference in ionic radius between the vacancy and the hydroxide ion causes a chemical expansion in the lattice when the material is hydrated [20].

The chemical expansion during hydration is a serious problem in applications with mechanical stress and fatigue that can cause micro cracking and deterioration of the material. Therefore, chemical expansion has been investigated, both

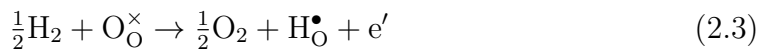
experimentally [21–23] and theoretically [24–28]. Despite the efforts to understand chemical expansion and thus the size difference between the vacancy and the proton, the size of the vacancy has been debated. The size of the oxygen vacancy is addressed in **Paper I**.

## 2.6 The oxyhydride barium titanate

Having studied the hydrogen in the state of a positively charged proton, the question naturally arises whether hydrogen can exist in other charged states in perovskites, such as the negatively charged hydride ion,  $\text{H}^-$  [29, 30]. It turns out that negatively charged hydride ions do exist in, e.g., oxyhydride phases, where a hydride ion is substituted on an oxygen site,  $\text{H}_\text{O}^\bullet$ . Oxyhydrides are rather rare in nature and until recently the layered perovskite structured  $\text{LaSrCoO}_3\text{H}_{0.7}$  and  $\text{SrCo}_2\text{O}_{4.33}\text{H}_{0.84}$  were the only reported transition metal oxides exhibiting higher than defect level amounts [31, 32]. The discovery of the oxyhydride perovskites  $(\text{Ca}, \text{Sr}, \text{Ba})\text{TiO}_{3-x}\text{H}_x$  was therefore rather unexpected [33, 34]. Among these BTO exhibits the highest amounts of hydrogen, up to  $x \lesssim 0.6$ .

The formation energy of a substitutional hydride ion is large and positive which implies that oxyhydride BTO is not thermodynamically stable and can form only under strongly reducing conditions provided by, e.g.,  $\text{CaH}_2$ . Nevertheless, it is kinetically stable in air (up to  $200^\circ\text{C}$ ) and under inert conditions up to  $450^\circ\text{C}$ , above which hydrogen gas is released [33]. The lattice constant increases slightly compared to the pristine lattice constant, and a phase transformation occurs from tetragonal to cubic. The substitutional hydride thus stabilises the cubic phase. In addition, oxyhydride BTO is a dark blue-black material, in contrast to white pristine BTO. The origin of the blue colour is not fully understood yet.

The substitutional hydrogen is stable only in the positive charge state ( $\text{H}_\text{O}^\bullet$ ) over the entire range of fermi levels within the bandgap [35, 36]. The formation reaction is thus



Therefore, it acts as a shallow donor contributing to  $n$ -type conductivity in the initially empty Ti  $3d$  band. Conductivity measurements confirm that  $\text{BaTiO}_{3-x}\text{H}_x$  is electrically conducting [33, 37]. However, while  $\text{SrTiO}_{3-x}\text{H}_x$  exhibits metallic-like conductivity over the whole concentration range,  $\text{BaTiO}_{3-x}\text{H}_x$  exhibits semiconductor-like conductivity at lower concentrations. At  $x = 0.14$  the conductivity in epitaxial thin films is semiconductor-like for all temperatures, at  $x = 0.24$  a semiconductor to metal transition occurs at 200 K, and at higher concentrations the conductivity is metallic for all temperatures [37]. This semiconductor-like conductivity has been attributed to the presence of small electron polarons forming a localised defect level in the bandgap [36].

## 2.7 Polaron as a quasi-particle

A band-state electron (or hole), i.e. an electron inside an allowed energy band, e.g., the conduction band, moves freely in the crystal with an effective mass,  $m^*$ , which differs from the electron mass in vacuum  $m_e$  [38, 39]. However, band theory follows from solving the electronic Hamiltonian in an assumed rigid lattice. In real materials the ions are mobile and at least in an ionic material an electron can polarise the lattice in its neighbourhood and localise. The combination of a localised, self-trapped electron with its accompanying lattice distortions can be treated as a quasi-particle called *polaron* [40–42].

If the extent of the polaron is large compared to the lattice spacing, the polaron is called large or Fröhlich polaron [40]. In this long wavelength limit the solid is treated in a continuum approximation in the adiabatic limit and the polaron moves around in the lattice with an increased effective mass compared to a bandstate electron.

A polaron with a radius for the lattice distortion of the order of the lattice spacing is called a small polaron. Hence, the charge carrier is often localised to a single atomic site. Figure 2.4 shows an example of a small polaron where the charge is localised almost entirely to one atom. Because of the short range of the small polarons the Fröhlich continuum theory is not applicable. Small polarons are on the other hand accessible through *ab initio* calculations. The small polaron can be described similar to a substitutional point defect and diffuses through the material through hopping between lattice sites [39].

The formation of a polaron from a delocalised bandstate electron is associated with an energy cost for the polarisation of the lattice. The energy gain by localising the electron must therefore be larger than the energy cost of the lattice polarisation to promote the the formation of a polaron. Figure 2.5 shows a schematic illustration of the energy as a function of lattice distortion. The formation energy  $E_{\text{pol}}$  is defined as the total energy difference between the relaxed polaronic and delocalised states, and is a combination of the strain energy required to distort the lattice  $E_{\text{st}}$  and the electronic energy gained by localising the electron in the distorted lattice,  $E_{\text{el}}$ .

In some cases the strain energy is too large compared to the electronic energy gain for the polaron to be favourable. Under such circumstances self-trapped electron polarons will not form. This is believed to be the case in pristine  $\text{BaTiO}_3$  [36]. A polaron can still form if strain can be induced by other means, e.g. by a charged point defect which attracts the polaron. The strain induced by the point defect lowers the strain energy required to form the polaron and a *bound polaron* is created.

Small self trapped electron polarons have been described in rutile  $\text{TiO}_2$  (although not in anatase) both theoretically [43–46] and experimentally [46–48]. The similarities between the electronic structure of  $\text{BaTiO}_3$  and  $\text{TiO}_2$  near the band edge suggests that the electronic properties should be similar, and that the difference

lies in the polarisability.

Bound polarons on the other hand have been discussed in BTO in connection with  $n$ -type doping such as  $\text{Nb}^{+5}$  substitution and oxygen vacancies [49, 50]. It is therefore plausible to assume that bound polarons could exist on the titanium ion in oxyhydride BTO where the natural associate defect site is the  $n$ -type  $\text{H}_\text{O}^\times$  defect [36].

Detection of polarons has proven a challenging task, both experimentally and theoretically. Due to the very short range of the lattice distortion, polarons cannot be seen from X-ray diffraction. Also the theoretical modelling of polarons in oxides has proven challenging. Density Functional Theory (cf. Section 5) with local and semi-local xc-functionals suffers from the well known self-interaction error which favours delocalisation of the electron and thus cannot properly describe charge localisation such as polarons. In **Paper II** we describe a method for polarons in *ab initio* calculations and how to characterise the bandstate from the polaron state using inelastic neutron scattering.

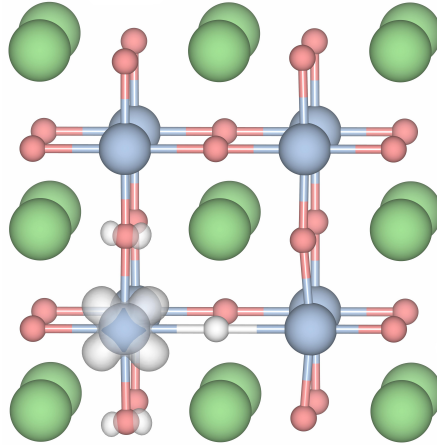


Figure 2.4: The polaron state of the oxyhydride phase of  $\text{BaTiO}_{3-x}\text{H}_x$  with a substitutional hydrogen on an oxygen site.

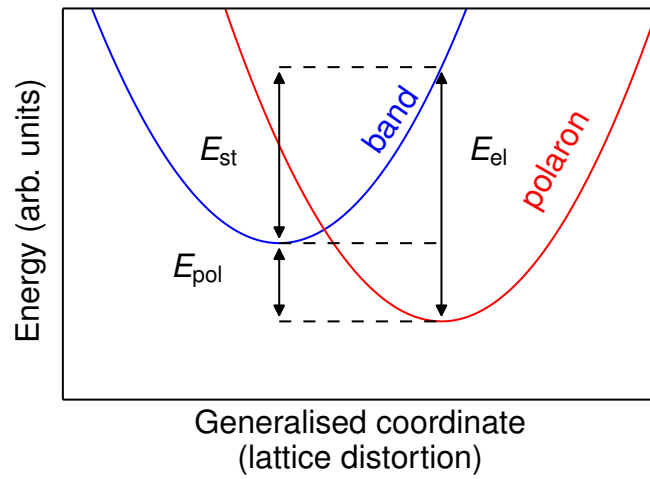


Figure 2.5: Schematic illustration showing the polaronic ( $E_{\text{pol}}$ ), lattice strain ( $E_{\text{st}}$ ), and electronic ( $E_{\text{el}}$ ) energies as a function of lattice distortion for the delocalised bandstate and the localised polaron state

## Energy of point defect formation

The formation of a point defect can be regarded as a chemical reaction which, at constant pressure,  $p$ , and temperature,  $T$ , proceeds in the direction that lowers the Gibbs free energy defined as

$$G = U + pV - TS = H - TS \quad (3.1)$$

where  $U$  is the internal energy,  $V$  the volume and  $S$  is the entropy.  $H$  is the enthalpy, defined as  $H = U + pV$ .

If we consider the formation of  $n$  independent defects the change in free energy can be written as

$$\Delta G = n\Delta_f G - T\Delta_f S_{\text{conf}} \quad (3.2)$$

where  $\Delta_f S_{\text{conf}}$  is the configurational entropy, the part of the entropy change associated with randomly distributing  $n$  defect in the material.  $\Delta_f G$ , the formation free energy for a single defect, can be written as

$$\Delta_f G = \Delta_f U + p\Delta_f V - T\Delta_f S \quad (3.3)$$

and is independent of the number of defects.

### 3.1 Formation energy

The formation free energy,  $\Delta_f G$ , can be separated into different contributions of chemical bonding and vibrational character [51]. The largest contribution is the formation energy,  $\Delta_f E$ , responsible for chemical bonding. The defect formation

energy for a defect  $X$  in charge state  $q$  is defined as [52, 53]

$$\begin{aligned} \Delta_f E [X^q] &= E_{\text{tot}} [X^q] - E_{\text{tot}} [\text{bulk}] + E_{\text{corr}}^q \\ &\quad - \sum_i \Delta n_i \bar{\mu}_i + q (\varepsilon_v + \mu_e + \Delta v_0) \end{aligned} \quad (3.4)$$

where  $E_{\text{tot}} [X^q]$  is the total energy at zero kelvin from a supercell calculation including the defect and  $E_{\text{tot}} [\text{bulk}]$  is the reference energy of the pristine material.  $E_{\text{corr}}^q$  is the energy correction which compensates for the spurious electrostatic interaction between charged defects in the supercell approach. There are several different correction schemes. **Paper II** makes use of the modified Makov-Payne correction scheme of Lany and Zunger [54]

$$\Delta E_{\text{corr}} = \frac{2}{3} \frac{Mq^2}{2\varepsilon L}, \quad (3.5)$$

where  $M$  is the Madelung constant,  $q$  is the charge,  $\varepsilon$  is the dielectric constant and  $L$  is the linear dimension of the supercell. The integer  $\Delta n_i$  is the number of atoms of type  $i$  that have been added ( $\Delta n_i > 0$ ) or removed ( $\Delta n_i < 0$ ) from the supercell in creating the defect, and  $\bar{\mu}_i$  is the corresponding chemical potential. The chemical potential  $\bar{\mu}_i$  is the reference energy of the reservoir with which the atoms are exchanged. If the reservoir is a gaseous phase the chemical potential can be computed from the expressions for a classical ideal gas. The electron chemical potential,  $\mu_e$ , is often called the Fermi energy and is customarily given relative to the valence band maximum,  $\varepsilon_v$ . The additional term  $\Delta v_0$  is used for properly aligning the electrostatic potentials of the bulk and the defect containing supercells [55, 56].

## 3.2 Chemical potentials for the gas phases

In a first approximation the chemical potentials for the gas phases  $\bar{\mu}_i$  can be taken as the total energies from electronic structure calculations similar to  $E_{\text{tot}} [X^q]$ . This is marked by a bar in Equation (3.4) and would correspond to the free energy at zero kelvin, neglecting zero point effects. At finite temperatures the pressure dependence for the gas phases can be assumed to follow classical ideal gas behaviour. The chemical potential for a mono atomic gas can then be written as

$$\mu_i(p_i, T) = \bar{\mu}_i + k_B T \ln \left( \frac{p_i V_Q}{k_B T} \right) \quad (3.6)$$

where  $k_B$  is Boltzmann's constant,  $p_i$  is the partial pressure and  $V_Q = (2\pi\hbar^2/mk_B T)^{3/2}$  is the quantum volume [53]. For molecules involving more than one atom additional

terms containing vibrational and rotational degrees of freedom must also be taken into account.

The vibrational contribution contains a temperature independent part, the zero point energy,  $\varepsilon^{\text{ZP}}$ , which can be separated from the temperature dependent part. If the zero-point energy is computed within the harmonic approximation the zero point energy is  $\varepsilon^{\text{ZP}} = \sum_k \hbar\omega_k/2$ , where  $\omega_k$  are the molecular vibrational frequencies. These frequencies can be obtained from tables [57] or computed with *ab initio* methods as described in Section 6.

The temperature dependence can be obtained by computing the full partition function, which is illustrated for the vibrational degrees of freedom in Section 3.3, but can also be taken, relative to the reference pressure  $p^\circ$ , from thermodynamic tables [58] if shifted such that  $h_i^\circ(0) = 0$ . The full pressure and temperature dependence of the chemical potential for the gas phases can, under the assumption of ideal gas behaviour, be written as

$$\mu_i(p_i, T) = \bar{\mu}_i + \varepsilon_i^{\text{ZP}} + h_i^\circ(T) - Ts_i^\circ(T) + k_{\text{B}}T \ln \left( \frac{p_i}{p^\circ} \right) \quad (3.7)$$

### 3.3 Vibrational free energy for the solid phases

Atoms in solids vibrate at characteristic frequencies related to the strength of the bond between the atoms which counter the displacement away from the equilibrium positions. In the harmonic approximation the restoring force follows Hooke's law and the potential is approximated to second order. Vibrations contribute to the free energy of the system and can be regarded as a correction to the formation energy in Equation (3.4). These contributions apply not only at finite temperature but, due to quantum mechanical effect, also at zero kelvin. Historically the vibrational contributions have often been neglected, partly due to the computational effort required [53].

The quantum mechanical energy for a harmonic oscillator is the given by

$$E_{ni} = \left( n + \frac{1}{2} \right) \hbar\omega_i \quad (3.8)$$

where  $n = 0, 1, 2 \dots$  is the quantum number, and  $\omega_i$  is the vibrational frequency. For a collection of independent harmonic oscillators with frequencies  $\omega_i$  the partition function is given by (with  $\beta = (k_{\text{B}}T)^{-1}$ )

$$Z_{\text{vib}} = \prod_i Z_i = \prod_i \sum_{n=0}^{\infty} e^{-\beta E_{in}} = \prod_i \frac{e^{-\beta\hbar\omega_i/2}}{1 - e^{-\beta\hbar\omega_i}} \quad (3.9)$$

The internal energy and the entropy can be obtained as derivatives of the partition function

$$U_{\text{vib}} = -\frac{\partial}{\partial\beta} \left( \ln Z_{\text{vib}} \right) = \sum_i \left( \frac{\hbar\omega_i}{2} + \frac{\hbar\omega_i}{e^{\beta\hbar\omega_i} - 1} \right) \quad (3.10)$$

$$S_{\text{vib}} = \frac{\partial}{\partial T} \left( k_B T \ln Z_{\text{vib}} \right) = k_B \sum_i \left( \frac{\beta\hbar\omega_i}{e^{\beta\hbar\omega_i} - 1} - \ln \left( 1 - e^{-\beta\hbar\omega_i} \right) \right) \quad (3.11)$$

The vibrational motion thus contributes both to the internal energy and the entropy.

### 3.3.1 Effect of constant pressure vs constant volume

Many defect calculations are performed at a constant volume under the assumption that the formation volume  $\Delta_f V$  in equation (3.3) in a solid is negligible. While this is true in general, the formation volume also affects other quantities indirectly, e.g. the relaxations around a point defect can cause significant changes to the vibrational properties and thus the formation entropy [59].

Although it is possible to compute the formation entropy directly through full vibrational calculations of the respective constant pressure systems, the constant (zero) pressure properties can be derived from the constant volume equivalent. The vibrational entropy at constant pressure can for example be written as [59–61]

$$\Delta_f S^{\text{vib}}(p=0) = \Delta_f S^{\text{vib}}(V_0) + \int_{V_0(T)}^{V^{p=0}(T)} \left( \frac{\partial S}{\partial V} \right)_T dV \quad (3.12)$$

Assuming that the integrand in the dilute limit only depends on the bulk properties it can be rewritten using the Maxwell relations [61, 62]

$$\left( \frac{\partial S}{\partial V} \right)_T = \left( \frac{\partial P}{\partial T} \right)_V = -V \left( \frac{\partial P}{\partial V} \right)_T \frac{1}{V} \left( \frac{\partial V}{\partial T} \right)_P = \beta_T \alpha_P \quad (3.13)$$

where  $\alpha_P$  and  $\beta_T$  are the isobaric thermal expansion and isothermal bulk modulus respectively and can be obtained from tables or, in the spirit of first principle, be computed from a series of phonon calculations at different volumes, i.e. the quasi-harmonic approximation [63, 64]. Assuming that  $\alpha_V$  and  $\beta_T$  are constant and unaffected by the defect formation the defect formation entropy at constant pressure for the defect  $X$  can be written as

$$\Delta_f S^{\text{vib}}[X](p=0) = \Delta_f S^{\text{vib}}(V_0)[X] + \alpha_V \beta_T \Delta_f V[X] \quad (3.14)$$

### 3.4 Configurational entropy

While the formation energy must be positive for the material to be stable the configurational entropy must be large enough to lower the free energy to a negative value to enable defect formation. Without the configurational entropy there would be no defect chemistry.

Unfortunately, the configurational entropy is by nature extremely difficult to calculate since each configuration has a probability of the respective Boltzmann factor. This means that the energy of every possible configuration must be computed in some way to give the probability of this configuration and thus the entropy. This can be done with cluster expansion in combination with Monte Carlo simulations and the Metropolis algorithm. However, since defect formation energies are often calculated in the dilute limit, i.e. in the limit where individual defects can be assumed to be independent of each other, it is possible to resort to a simpler first approximation to the configurational entropy, the ideal solution where all configurations have the same probability.

For  $n$  defects distributed on  $N$  sites with a degeneracy factor  $m$  accounting for the internal degrees of freedom of the point defect, the number of microstates is

$$\Omega = \frac{mN \cdot m(N-1) \cdots m(N-n+1)}{n} = m^n \binom{N}{n} \quad (3.15)$$

and the entropy can be written with the use of Stirling's approximation as

$$S = k_B \ln \Omega \approx n \ln m + N \ln \frac{N}{N-n} - n \ln \frac{n}{N-n} \quad (3.16)$$

Since  $\Omega \geq 1$  and  $T$  are always positive, the configurational formation entropy contribution to the free energy is always negative, thus favouring defect formation.

In the dilute limit the total free energy change  $\Delta G$  is a function of the number of defects  $n$  only through the configurational entropy and can now be written as in Equation (3.2), restated here for convenience

$$\Delta G = n\Delta_f G - TS^{\text{conf}}(n) \quad (3.2)$$

An equilibrium is obtained when the derivative with respect to the number of defects is zero. The equilibrium condition then reads

$$\begin{aligned} \frac{\partial G}{\partial n} &= \frac{\partial}{\partial n} \Delta G \\ &= \Delta_f G + k_B T \left( \ln \frac{n}{N-n} - \ln m \right) = 0 \end{aligned} \quad (3.17)$$

It is convenient to introduce the defect concentration  $x = n/N$ . The equilibrium concentration is then given by

$$\frac{x_{\text{eq}}}{1 - x_{\text{eq}}} = m e^{-\Delta_f G/k_B T} \quad (3.18)$$

If one of the constituent elements is exchanged with a gas phase the pressure dependence can be written out explicitly using Equation (3.7) and the equilibrium concentration is given by

$$\frac{x_{\text{eq}}}{1 - x_{\text{eq}}} = m \left( \frac{p_i}{p^\circ} \right) e^{-\Delta_f G^\circ/k_B T} \quad (3.19)$$

where  $\Delta_f G^\circ$  is the formation free energy at the reference pressure  $p^\circ$ .

## Chemical expansion

While the formation volume contribution to the formation free energy is negligible, the formation volume is significant when it comes to chemical expansion. As already mentioned in Section 2.5 the formation volume induces strain in the material upon defect formation. In a material where the composition changes constantly, such as in a proton conducting fuel cell membrane where the material is constantly hydrated and de-hydrated, this is particularly important. Chemical expansion is often measured as a unit cell volume change per defect, or per water molecule. This works well in (pseudo) cubic material where the strain can be considered isotropic, but does not capture the anisotropy or shear that a single defect may induce. To model this we have expressed the chemical expansion in terms of defect induced strain tensor in **Paper I**. Although it turned out that the strain tensors indeed were diagonal **Paper I** is written with just such a general case in mind.

### 4.1 A thermodynamics view on strain

Let us consider the crystal volume,  $V = V(T, P, \{x_k\})$ , to depend on the temperature, pressure and defect concentration of species  $k$ . In analogy with the thermal expansion coefficient and the bulk modulus mentioned above we now define the chemical expansion coefficient as [20]

$$\beta_k = \frac{1}{V} \left( \frac{\partial V}{\partial x_k} \right)_{P, T, x_{k'} \neq x_k} \quad (4.1)$$

In order to generalise the scalar chemical expansion coefficient to three dimensions, we first note that the volume expansion of a material in the small strain limit is

given by the trace of the strain tensor [65,66]

$$\frac{\Delta V}{V} = \text{Tr}(\varepsilon) \quad (4.2)$$

By dividing by the change in defect concentration  $\Delta x_k$  and taking the infinitesimal limit we can write the chemical expansion coefficient as

$$\beta_k = \text{Tr} \left( \frac{\partial \varepsilon}{\partial x_k} \right)_{P,T,x_{k'} \neq x_k} = \text{Tr}(\lambda_k)_{P,T,x_{k'} \neq x_k} \quad (4.3)$$

where  $\lambda$  is the *defect induced strain tensor* in the infinite dilute limit [67].

## 4.2 The defect induced strain tensor

The defect induced strain tensor is the natural generalisation of the chemical expansion coefficient. In practical calculations with a finite concentration, we consider the effect of a single defect introduced in a volume  $V_0$ . With a defect concentration  $x_d = \Omega_c/V_0$ , where  $\Omega_c$  is the volume of a primitive unit cell, the defect induced strain tensor is

$$\lambda = \frac{1}{x_d} \varepsilon \quad (4.4)$$

With this definition we get the chemical expansion coefficient as

$$\beta = \text{Tr}(\lambda) = \frac{1}{x_d} \text{Tr}(\varepsilon) = \frac{V_0}{\Omega_c} \cdot \frac{\Delta V}{V_0} = \frac{\Delta V}{\Omega_c} \quad (4.5)$$

and the defect formation volume is given by

$$\Delta_f V = \Omega_c \text{Tr}(\lambda) \quad (4.6)$$

## 4.3 Strain in one dimension

The strain tensor appearing in Equations (4.3) and (4.4) is often calculated from the relative lattice expansion, the linear strain, for each axis in the crystal. In an isotropic cubic material in which the defects can be assumed to be randomly oriented, causing no shear strain, the linear strains are all equal and are found along the diagonal in the three dimensional strain tensor. With the volume expansion in Equation (4.2) equal to the trace of the strain tensor the volume expansion can be written as three times the linear strain.

Consider therefore a one-dimensional object of initial length  $l_0$ . This can e.g. be the lattice constant in a cubic material. It is, by some means, forced into a new length  $l$ , which can be either larger or smaller than  $l_0$ . The elongation

$$\Delta l = l - l_0 \quad (4.7)$$

is defined such that it is positive (negative) if the length of the rod has increased (decreased). The strain is the dimensionless quantity

$$e = \frac{\Delta l}{l_0} \quad (4.8)$$

This is called the *engineering strain* [68] and is the measured quantity in an experiment. There is, in general, no reason to favour  $l_0$  over  $l$  in the denominator and the engineering strain can just as well be defined with  $l$  in place of  $l_0$ . To relate the elongation to the original length of the rod, i.e. using  $l_0$  in the denominator, is called the *Lagrangian strain measure* and relating the elongation to the final length,  $l$ , is called *Eulerian strain measure* [68].

Under the assumption that the strain is small the Lagrangian strain and the Eulerian strain are approximately equal, but under greater strain one would ideally measure the length  $l$  at every infinitesimal  $\Delta l$  in order to compute the logarithmic or *true strain*. The true strain is defined as

$$e = \int_{l_0}^l \frac{dl'}{l'} = \ln \left( \frac{l}{l_0} \right) \approx \frac{l - l_0}{l_0} \quad (4.9)$$

where the last approximation is valid under small strain and takes us back to the engineering strain. The one-dimensional engineering strain is the average of the diagonal terms in the full strain tensor  $e = \text{Tr}(\varepsilon)/3$  and the chemical expansion coefficient can now be computed as

$$\beta = 3 \frac{\Delta l/l_0}{x_d} = \frac{3e}{x_d} \quad (4.10)$$

## 4.4 The strain tensor

When there is shear strain present, or when the crystal is not cubic the linear strain is not sufficient to describe the deformation of the crystal. Under such circumstances a formalism for a three dimensional body has to be used.

Assume a body in three dimensions can be described as a periodic lattice with a unit cell of basis vectors  $\mathbf{a}_1$ ,  $\mathbf{a}_2$  and  $\mathbf{a}_3$ . Let

$$\mathbf{a}_i = L_0 \mathbf{e}_i \quad (4.11)$$

be the one-to-one matrix transformation that maps the cartesian coordinates  $\mathbf{e}_i$  onto the undeformed crystal  $\mathbf{a}_i$ . After deformation the crystal is defined by the new set of basis vectors

$$\mathbf{a}'_i = \mathbf{L} \mathbf{e}_i = \mathbf{L}\mathbf{L}_0^{-1}\mathbf{a}_i \quad (4.12)$$

The last equality follows because  $\mathbf{L}_0$  is one-to-one and Equation (4.11) is invertible.

The location of an arbitrary point  $P = (p_1, p_2, p_3)$  as measured relative to the cell vectors in the undeformed crystal can be written as

$$\mathbf{r} = \sum_i p_i \mathbf{a}_i \quad (4.13)$$

and analogously after deformation. The displacement of the point is

$$\mathbf{u} = \mathbf{r}' - \mathbf{r} = \sum_i p_i (\mathbf{a}'_i - \mathbf{a}_i) = (\mathbf{L}\mathbf{L}_0^{-1} - \mathbf{1}) \mathbf{r} \quad (4.14)$$

The linear transformation  $\mathbf{F} = \mathbf{L}\mathbf{L}_0^{-1}$  that maps the undeformed system onto the deformed is called the displacement gradient and can formally written as

$$\mathbf{F} = \frac{\partial r'_i}{\partial r_j} \quad (4.15)$$

from which the Biot strain tensor is defined as

$$\varepsilon_{ij} = \frac{\partial u_i}{\partial r_j} = \frac{\partial (r'_i - r_i)}{\partial r_j} = \frac{\partial r'_i}{\partial r_j} - \delta_{ij} = \mathbf{F} - \mathbf{1} \quad (4.16)$$

We can now recognise

$$\varepsilon = (\mathbf{L}\mathbf{L}_0^{-1} - \mathbf{1}) \quad (4.17)$$

in Equation (4.14) as the Biot strain tensor in the Lagrangian description of continuum mechanics.

A transformation of a three dimensional body can in general be decomposed in three different actions; translation, rotation and deformation. Translation, as well as rotation, can have no thermodynamical significance, since they do not alter the internal structure of the body. Translation are by construction not included. Rotations on the other hand can in principle be present since the Biot strain tensor is not by necessity symmetric.

Rotations can be removed through a symmetrization procedure. In general this can be done through a polar decomposition [68], but for small rotations it is sufficient to add the transpose and take the mean. The strain tensor is then given by

$$\varepsilon_{ij} = \frac{1}{2} \left( \frac{\partial u_i}{\partial r_j} + \frac{\partial u_j}{\partial r_i} \right) \quad (4.18)$$

or in matrix notation

$$\varepsilon = \frac{1}{2} \left( \mathbf{L}\mathbf{L}_0^{-1} + (\mathbf{L}_0^{-1})^T (\mathbf{L})^T \right) \quad (4.19)$$

However, if no rotations are present there is no reason to favour one strain tensor over another and the strain tensor can be computed as the Biot strain tensor

$$\varepsilon = (\mathbf{L}\mathbf{L}_0^{-1} - \mathbf{1}) = (\mathbf{L} - \mathbf{L}_0) \mathbf{L}_0^{-1} \quad (4.20)$$

This is the natural generalisation of the engineering strain in Equation (4.8) to three dimensional objects.



## Electronic structure calculations

The present thesis uses so called first principles or *ab initio* methods to compute relevant quantities. At the core of first principles calculations is the absence of experimentally fitted parameters. All derived and computed quantities should be obtained *ab initio*, i.e. from the fundamental description of the nature, the Schrödinger equation. The full time-independent Schrödinger equation in its most compact form reads

$$\mathcal{H}\Psi(\mathbf{x}, \mathbf{R}) = E\Psi(\mathbf{x}, \mathbf{R}) \quad (5.1)$$

where  $\mathcal{H}$  is the Hamiltonian,  $\Psi$  is the (multi-particle) wavefunction,  $E$  is the energy eigenvalues,  $\mathbf{R}$  are the positions of the ions and  $\mathbf{x}$  the position and spin of the electrons. Almost all *ab initio* calculations rely on the separation of the full Hamiltonian into one electronic Hamiltonian and one ionic Hamiltonian. The justification for this is the almost instantaneous electronic response to an ionic displacement due to the much lower mass of the electrons. The instantaneous response implies that, as far as electron degrees of freedom are concerned, the ionic position can be treated parametrically. This is called the Born-Oppenheimer or *Adiabatic Approximation*.

After a justification of the adiabatic approximation, the present chapter gives an overview of the methods used for solving the electronic structure problem [69–76]. The ionic motion is treated in Chapter 6.

## 5.1 Adiabatic Approximation

For a multi-particle system the full Hamiltonian<sup>1</sup> reads

$$\mathcal{H} = - \sum_{i=1}^N \frac{\nabla_i^2}{2} - \sum_{k=1}^K \frac{\nabla_k^2}{2M_k} + \frac{1}{2} \sum_{\substack{i,j=1 \\ i \neq j}}^N \frac{1}{|\mathbf{r}_i - \mathbf{r}_j|} - \sum_{k=1}^K \sum_{i=1}^N \frac{Z_k}{|\mathbf{r}_i - \mathbf{R}_k|} + \frac{1}{2} \sum_{\substack{k,k'=1 \\ k \neq k'}}^K \frac{Z_k Z_{k'}}{|\mathbf{R}_k - \mathbf{R}_{k'}|} \quad (5.2)$$

where upper case denotes ionic and lower case electronic quantities. The terms represent in order, the kinetic energy for the electrons and nuclei (with mass  $M_k$ ), the interaction between electrons, between electrons and nuclei and between the nuclei.

With the electronic Hamiltonian in the adiabatic approximation defined as

$$\mathcal{H}_{el} = \sum_i \left[ -\frac{\nabla_i^2}{2} + V_{ext}(\mathbf{r}_i) \right] + \frac{1}{2} \sum_{i \neq j} \frac{1}{|\mathbf{r}_i - \mathbf{r}_j|} \quad (5.3)$$

where

$$V_{ext}(\mathbf{r}_i) = - \sum_k \frac{Z_k}{|\mathbf{r}_i - \mathbf{R}_k|} \quad (5.4)$$

is the external potential caused by the ions, the Schrödinger equation for the electrons with the ions at positions  $\mathbf{R}$  can be written

$$\mathcal{H}_{el}\psi_{\mathbf{R}}(\mathbf{r}) = \varepsilon_{\mathbf{R}}\psi_{\mathbf{R}}(\mathbf{r}) \quad (5.5)$$

The solution to the electronic Hamiltonian will be discussed in this chapter.

The remaining terms in the full Hamiltonian in Equation (5.2) form in the ionic Hamiltonian

$$\mathcal{H}_{ion} = - \sum_k \frac{\nabla_k^2}{2M_k} + V(\mathbf{R}) \quad (5.6)$$

where  $V(\mathbf{R})$  is the potential created by the combination of the repulsive ionic potential and the chemical bonding from the electrons. This is treated in Section 6.

Even when applying the adiabatic approximation the multi-electron Schrödinger equation in Equation (5.5) is quite intractable. Several methods for solving the electronic structure problem have been utilised over the years [74, 75]. The intuitively most accessible is perhaps the Hartree-Fock (HF) approximation. The HF

<sup>1</sup>In atomic units in which  $\hbar = e = m_e = 1/(4\pi\epsilon_0) = 1$ .

approximation is also the foundation for understanding notions such as the Hartree potential, self-interaction error and exact exchange, which is used in hybrid functionals in DFT. In addition, many conclusions and technical aspects carry over to DFT.

## 5.2 The Hartree-Fock approximation

A first approximation to the electronic structure problem can be made by approximating the full wave function with the product of single particle wave functions  $\Psi(\mathbf{x}_1, \mathbf{x}_2, \dots, \mathbf{x}_N) = \psi_1(\mathbf{x}_1)\psi_2(\mathbf{x}_2)\dots\psi_N(\mathbf{x}_N)$ , where  $\psi_i$  are one particle wave functions and  $\mathbf{x}_i = \mathbf{x}_i(\mathbf{r}_i, \sigma_i)$  denotes the position  $\mathbf{r}_i$  and the spin  $\sigma_i$ . This is sometimes referred to as the Hartree approximation. However, this does not respect the anti-symmetry of the wave function required by permutation symmetry for fermions. This can be accounted for in the shape of a *Slater determinant*

$$\Psi(\mathbf{x}_1\mathbf{x}_2\dots\mathbf{x}_N) = \frac{1}{\sqrt{N!}} \begin{vmatrix} \psi_1(\mathbf{x}_1) & \psi_2(\mathbf{x}_1) & \cdots & \psi_N(\mathbf{x}_1) \\ \psi_1(\mathbf{x}_2) & \psi_2(\mathbf{x}_2) & \cdots & \psi_N(\mathbf{x}_2) \\ \vdots & \vdots & \ddots & \vdots \\ \psi_1(\mathbf{x}_N) & \psi_2(\mathbf{x}_N) & \cdots & \psi_N(\mathbf{x}_N) \end{vmatrix} \quad (5.7)$$

where the  $\psi_i(\mathbf{x}_j)$  is the atomic orbital of atom  $i$  at position  $\mathbf{r}_j$  with spin  $\sigma_j$ . The introduction of spin here is necessary since the total wave function consists of both a spatial and a spin part. In order for the total wavefunction to be anti-symmetric, as required for fermions, the contributions from both spin and spatial parts need to be considered. When the spin part is symmetric the spatial wavefunction must be corrected for the self-interaction error with the inclusion of exchange as discussed below.

The single particle wave functions are optimised using the variational principle. By the variational principle the expectation value of the Hamiltonian is always higher than the true ground state energy

$$E_0 \leq \frac{\langle \Psi | \mathcal{H} | \Psi \rangle}{\langle \Psi | \Psi \rangle} \quad (5.8)$$

for any wave function  $\Psi$ , with equality for the true ground state  $|\Psi_0\rangle$ . The ground state is obtained by minimising the energy with respect to the wavefunction  $\Psi$  subject to the constraint

$$\int d\mathbf{r} n(\mathbf{r}) = \int d\mathbf{r} \sum_{i=1}^N n_i(\mathbf{r}) = \int d\mathbf{r} \sum_{i=1}^N \sum_{\sigma} |\psi_i(\mathbf{r}, \sigma)|^2 = N \quad (5.9)$$

where  $n(\mathbf{r})$  is the electron density and  $N$  is the number of electrons. The Hartree-Fock (HF) equation for the single particle state  $\psi_i$  then becomes

$$\begin{aligned} \left[ -\frac{1}{2}\nabla^2 + V_{ext}(\mathbf{r}) \right] \psi_i(\mathbf{x}) + \sum_{j=1}^N \int d\mathbf{x}' |\psi_j(\mathbf{x}')|^2 \frac{1}{|\mathbf{r} - \mathbf{r}'|} \psi_i(\mathbf{x}) \\ - \sum_{j=1}^N \int d\mathbf{x}' \psi_j^*(\mathbf{x}') \frac{1}{|\mathbf{r} - \mathbf{r}'|} \psi_i(\mathbf{x}') \psi_j(\mathbf{x}) = \varepsilon_i \psi_i(\mathbf{x}) \end{aligned} \quad (5.10)$$

The total energy in the HF approximation is obtained as

$$E_{HF} = -\frac{1}{2} \sum_i \int \psi_i^*(\mathbf{r}) \nabla^2 \psi_i(\mathbf{r}) d\mathbf{r} + \int V_{ext}(\mathbf{r}) n(\mathbf{r}) d\mathbf{r} + E_H + E_x \quad (5.11)$$

or in terms of the eigenvalues as

$$E_{HF} = \sum_i \varepsilon_i - E_H - E_x \quad (5.12)$$

The first two terms in Equation (5.11) are the kinetic energy and the energy from the external potential from by the nuclei. The third term

$$E_H = \frac{1}{2} \iint \frac{n(\mathbf{r}') n(\mathbf{r})}{|\mathbf{r} - \mathbf{r}'|} d\mathbf{r}' d\mathbf{r} \quad (5.13)$$

is called the Hartree energy and contains the interaction from the average charge distribution caused by all the electrons. The Hartree term introduces an interaction between an electron and the electron density of the crystal, which in turn contains the electron itself. The electron thus interacts with itself. This causes the so called *self-interaction error*. The fourth term

$$E_x = -\frac{1}{2} \sum_{j=1}^N \delta_{\sigma_i, \sigma_j} \int d\mathbf{r} d\mathbf{r}' \psi_i^*(\mathbf{r}) \psi_j^*(\mathbf{r}') \frac{1}{|\mathbf{r} - \mathbf{r}'|} \psi_i(\mathbf{r}') \psi_j(\mathbf{r}) \quad (5.14)$$

is the non-local exchange term and is the result of the anti-symmetry of the wave function. The exchange term, which is non-zero only if the spin are parallel, removes the self-interaction. HF is thus (one-particle) self-interaction free. However, the true wavefunction is not a single particle theory and HF is not many-particle self-interaction free, as will be discussed below.

The difference between the Hartree and the Hartree-Fock approximations is the inclusion of *exchange* which removes the self-interaction caused by the Hartree term. Still, HF is an approximation and by definition the difference between the true many-particle ground state energy and the HF energy is called *correlation* [77].

## 5.3 The Hohenberg-Kohn Theorems

The great advantage of the HF Equation (5.10) is that the  $N$ -multiparticle Schrödinger equation has been reduced to  $N$  non-interacting single state equations. The great disadvantages are that correlation has been left out, that the exchange term is non-local and that information about all single particle wave functions has to be stored. However, the problem can be reformulated with the electron density as the fundamental variable. This possibility of using the density as a fundamental variable had been explored [74–76], first by Thomas [78], Fermi [79] and Dirac [80] and also extensively in the special case of the homogeneous electron gas before Hohenberg and Kohn [81] proved in two famous theorems that

1. the external potential  $V_{\text{ext}}$  and thus the full Hamiltonian is uniquely determined by the ground state density  $n_0(\mathbf{r})$
2. there exists a functional  $E[n, V_{\text{ext}}]$  for any external potential  $V_{\text{ext}}$  such that the electron density  $n(\mathbf{r})$  that minimises this functional will be the exact ground state density.

In short this means that there exists a functional of the electron density only, for any external potential, which solves the problem exactly, not only including exchange but also correlation. Furthermore, it uses the electron density as the fundamental variable.

The functional is defined by Hohenberg and Kohn as

$$F_{HK}[n] = \langle \Psi | T + V_{ee} | \Psi \rangle \quad (5.15)$$

where  $T$  is the kinetic energy and  $V_{ee}$  electron-electron interaction of the full interacting system. The corresponding energy functional

$$E_{HK}[n] = F[n] + \int d\mathbf{r} V_{\text{ext}}(\mathbf{r})n(\mathbf{r}) \quad (5.16)$$

satisfies the variational principle, i.e. it assumes its minimum at the value for the correct electron density  $n(\mathbf{r})$  subject to the constraint

$$\int n(\mathbf{r})d\mathbf{r} = N \quad (5.17)$$

Unfortunately, the Hohenberg-Kohn theorems give no explicit expression for this functional. While the last term in Equation (5.16) is easily computed, the Hohenberg-Kohn functional  $F_{HK}[n]$ , containing the kinetic energy and the electron-electron interaction of the full interacting system, remains unknown.

## 5.4 The Kohn-Sham Approach

Despite the theoretical beauty of the Hohenberg-Kohn theorems they provide no recipe for how to make use of these theorems. An ansatz was proposed by Kohn and Sham [82] in which the full interacting many-body system is replaced by an auxiliary system of independent particles. The ansatz relies heavily on the first Hohenberg-Kohn theorem which can be regarded as the inverse relation to the Schrödinger equation. While the Schrödinger equation uniquely determines the wave functions and thus the electron density for a given external potential the first Hohenberg-Kohn theorem proves that the inverse relation also holds.

The great benefit of the auxiliary system is twofold; firstly, it reduces the full problem of  $N$  interacting particles to  $N$  single particle systems, secondly, it separates out the kinetic energy term and the long-range Hartree term in such a way that the remaining exchange-correlation (xc) term can be approximated reasonably well by local or nearly local functionals of the density.

It should be stressed that the Kohn-Sham approach is *not* an approximation. In theory the Kohn-Sham approach would be exact if only the exchange-correlation functional were known. However, for practical calculations approximations to the unknown exchange-correlation functional must be introduced.

## 5.5 The Kohn-Sham equations

Kohn-Sham, in a manner analogous to the Hartree-Fock approximation, proposed a separation of the two first terms into three terms; a kinetic energy term of a *non*-interacting single particle  $T_s[n(\mathbf{r})]$ , a Hartree term  $E_H[n(\mathbf{r})]$  and an exchange-correlation term  $E_{xc}$ . The Hohenberg-Kohn energy functional in Equation (5.16) in the Kohn-Sham ansatz then becomes

$$E_{KS}[n] = T_s[n(\mathbf{r})] + E_H[n(\mathbf{r})] + E_{xc}[n(\mathbf{r})] + \int d\mathbf{r} V_{ext}(\mathbf{r})n(\mathbf{r}) \quad (5.18)$$

A variation of this expression with respect to the single particle wave functions  $\psi_i(\mathbf{r})$  subject to the constraint in Equation (5.17) leads to

$$\left[ -\frac{1}{2}\nabla^2 + \int \frac{n(\mathbf{r}')}{|\mathbf{r} - \mathbf{r}'|} d\mathbf{r}' + V_{xc}(\mathbf{r}) + V_{ext}(\mathbf{r}) \right] \psi_i(\mathbf{r}) = \varepsilon_i \psi_i(\mathbf{r}) \quad (5.19)$$

where

$$V_{xc}(\mathbf{r}) = \frac{\delta E_{xc}[n(\mathbf{r})]}{\delta n(\mathbf{r})} \quad (5.20)$$

The total energy of the system is

$$E_{KS} = \sum_i \varepsilon_i - E_H[n(\mathbf{r})] + E_{xc}[n(\mathbf{r})] - \int d\mathbf{r} V_{xc}[n(\mathbf{r})]n(\mathbf{r}) \quad (5.21)$$

Although the Kohn-Sham ansatz Equation (5.19) is similar to the Hartree-Fock Equation (5.10) the main difference is, apart from that correlation is now included albeit not known, that the Hamiltonian now depends on the density and not the one-particle wavefunctions.

## 5.6 Approximations to the Exchange-Correlation Functional

Up to this point the Density Functional Theory is exact, save for the adiabatic approximation, but since the xc-functional in Equation (5.20) is unknown it has to be approximated in some way. The Kohn-Sham approach of separating the Hohenberg-Kohn functional  $F_{HK}$  in a kinetic energy, a long range Hartree term and an exchange-correlation (xc) functional  $E_{xc}$  has the advantage that the xc-functional is rather small compared to the kinetic and the Hartree energies and may be approximated reasonably well as a local or nearly local functional of the particle density at the point  $\mathbf{r}$ . The accuracy of any DFT-calculation relies on the approximations of the xc-functional. Over the years an abundance of different xc-functional approximations have been proposed [74, 83], but still today the original functional proposed by Kohn-Sham, the local density approximation, is competitive in certain areas.

### 5.6.1 Local Density Approximation

The local density approximation (LDA) is perhaps the least sophisticated xc-functional. It is based upon the assumption that the electronic structure in solids to a good approximation can be described by the homogeneous electron gas [82]. In this limit the exchange and correlation for a homogeneous electron gas is local, i.e. depends only on the electron density at each point, and can be given an analytical expression, although the coefficients must be computed using quantum Monte Carlo techniques [77, 84–86]. The total xc-functional in the local density approximation can then be written as

$$E_{xc}[n(\mathbf{r})] = \int d\mathbf{r} n(\mathbf{r}) \varepsilon_{xc}(n(\mathbf{r})) \quad (5.22)$$

where  $\varepsilon_{xc}(n(\mathbf{r}))$  is the energy density per electron at a point  $\mathbf{r}$ .

This approximation is remarkably accurate for many solids and was a contributing factor to the great success of the density functional theory. In particular the LDA predicts e.g. bond lengths in solids with close to homogeneous electron density to within a few percent. However, the LDA fails in molecules where the density varies rapidly.

## 5.6.2 Generalised Gradient Approximation

The general success of the LDA has inspired the development of various Generalised Gradient Approximations (GGA) with the explicit aim of accounting for the inhomogeneous electron density found in real material. The natural extension of the LDA is to include not only the (local) density at a point  $\mathbf{r}$  but also (semi-local) gradients of the density  $\varepsilon_{xc} = \varepsilon_{xc}(n(\mathbf{r}), \nabla n(\mathbf{r}))$ . The presence of gradients in the functional expression have given this class of functionals its name. Several various forms have been proposed and although derived in different manners the GGA:s give similar improvements over LDA. Among the most famous are the GGA proposed by Perdew and Wang (PW91) [85] and Perdew, Burke and Ernzerhof [87,88] (PBE) of which the latter has been used in both **Paper I** and **Paper II**.

## 5.6.3 Hybrid functionals

DFT suffers from the well known self-interaction problem [77] caused by the Hartree potential, as mentioned in Section 5.2. In the absence of exact exchange this self interaction is not removed. Self interaction leads to a deviation from piecewise linearity of the xc-functional, a theoretically known property of the exact xc-functional, and delocalisation of the electrons.

It was mentioned originally by Kohn and Sham that the inclusion of exact exchange (EX), i.e. exchange computed using the Hartree-Fock method, should improve the results compared to LDA since, although correlation is approximated, at least exchange is included exactly. As Kohn and Sham point out this may be regarded as a Hartree-Fock method corrected for correlation.

The expected improvement over local and semi-local xc-functionals have inspired a number of functionals incorporating EX. However, although the inclusion of exact exchange is supposed to remove the self-interaction this is not the case. While the Hartree-Fock method is one-electron self-interaction-free it is not many-electron self-interaction-free and thus over-compensates the self-interaction [53]. Therefore, in general, EX is not incorporated in the way that was proposed by Kohn and Sham but by mixing a fraction of EX with the DFT exchange

$$E_{xc} = E_{xc}^{\text{DFT}} + \alpha (E_x^{\text{HF}} - E_x^{\text{DFT}}) \quad (5.23)$$

One popular choice based on theoretical arguments is the mixing proposed by Perdew, Ernzerhof and Burke (PBE0) [89], which mixes the exchange and correlation from the GGA-PBE with 25% EX.

A computationally more efficient functional is the range separated hybrid functional proposed by Heyd, Scuseria and Ernzerhof (HSE) [90, 91] which splits the terms in the PBE0 into short- and long-range components, with EX only included within the region defined by the parameter  $\omega$  and the long range exchange given

by the semi-local PBE exchange.

$$E_{xc}^{\text{HSE}} = aE_x^{\text{HF,SR}}(\omega) + (1 - a)E_x^{\text{PBE,SR}}(\omega) + E_x^{\text{PBE,LR}}(\omega) + E_c^{\text{PBE}} \quad (5.24)$$

The adjustable parameter  $\omega$ , determines the extent of the short-range interactions, with  $\omega = 0$  is equivalent to PBE0 and  $\omega \rightarrow \infty$  to PBE. The  $\omega$  must be small enough to agree with PBE0, but large enough to increase performance. There are two standard choices of  $\omega$ . The first published article (HSE03) [90] stated a value of  $\omega = 0.15^{1/4} a_0^{-1} = 0.3 \text{ \AA}^{-1}$ . However, this was not the value actually used in the article and later an erratum was published [91] with stated a value of  $\omega = 0.2 \text{ \AA}^{-1}$ . The latter functional, which goes under the name HSE06, has been used in **Paper II**.

#### 5.6.4 DFT+ $U$ – “poor man’s hybrid”

Calculations of exact exchange is computationally very demanding and sometimes the desired properties can be obtained with simpler methods. While hybrids are necessary for correcting the underestimated band-gap in a DFT calculation, the bandstructure within occupied bands can be improved by less computationally demanding schemes such as the DFT+ $U$  method [53, 92–94].

As opposed to the rather delocalised  $s$  and  $p$  states, the  $d$  and  $f$  states are rather localised and are not well described by LDA or GGA, which favour fractional occupancies. By adding a Hubbard-like on-site repulsion term to the semicore  $d$  (of  $f$ ) states, fractional occupancies are penalised and the total energy is written [53]

$$E_{\text{tot}}^{\text{DFT}+U}[\rho(\mathbf{r})] = E_{\text{tot}}^{\text{DFT}}[\rho(\mathbf{r})] + \sum_t \frac{U}{2} \left( \sum_{\alpha,\sigma} n_{\alpha,\alpha}^{t,\sigma} - \sum_{\alpha,\beta,\sigma} n_{\alpha,\beta}^{t,\sigma} n_{\beta,\alpha}^{t,\sigma} \right) \quad (5.25)$$

where  $n_{\alpha,\alpha}^{t,\sigma}$  are the occupation matrices involving orbitals  $\alpha$  and  $\beta$  for site  $t$  and spin channel  $\sigma$ .

The value of the  $U$  parameter is not transferable and has to be determined from case to case. Different possible approaches for determining the  $U$  parameter are possible, e.g. to produce the correct bandgap or the correct position of the  $d$ -band [95]. In the spirit of *first principles* it is desirable to determine the value of  $U$  without relying on experimental observations. In **Paper II** we choose to fit the  $U$  parameter to the piecewise linearity constraint of the xc-functional, i.e. that the energy increases linearly when filling the defect level, which is a theoretically known property of the true xc-functional [96].

## 5.7 Implementation in periodic solids

The presence of a differential operator in the Schrödinger equation Hamiltonian has caused a wide variety of approaches concerning the practical implementation. One of the most important aspects is how to represent the trial wavefunction solutions. A common approach is to expand the wavefunction in a complete set of basis functions, e.g. in a linear combination of atomic orbitals, which is rather natural in the representation of isolated molecules.

In solids with periodic boundary conditions the natural basis function is the plane wave due to its intrinsic periodicity. In a planewave basis an important implementation aspect is how to represent the core and the core electrons. A proper description of the core, where the wavefunctions oscillate rapidly, requires a very large number of plane waves. The all-electron potentials are not well suited for a planewave basis set, but by constructing an effective potential the core electrons, which do not participate in chemical bonding, can be treated together with the nuclei in a pseudopotential. The resulting system will exhibit a much smoother potential requiring significantly fewer planewave basis functions. With the PAW method the all-electron properties can still be obtained.

Since VASP, which is the code used throughout this thesis, is a planewave PAW code, these aspects will be given attention in the following sections.

### 5.7.1 Plane waves

Consider a lattice with the periodicity  $\mathbf{R}$ . The effective potential is then also periodic with the same periodicity  $v_{\text{eff}}(\mathbf{r}) = v_{\text{eff}}(\mathbf{R} + \mathbf{r})$ . In such a periodic lattice Bloch's theorem states that a one-electron wavefunction can be written as

$$\psi_{\mathbf{k}}(\mathbf{r}) = u_{\mathbf{k}}(\mathbf{r})e^{i\mathbf{k}\cdot\mathbf{r}} \quad (5.26)$$

where  $u_{\mathbf{k}}(\mathbf{r})$  is a function with the periodicity of the lattice. Like any periodic function it can be expanded in a Fourier series

$$u_{\mathbf{k}}(\mathbf{r}) = \sum_m c_{\mathbf{k},m} e^{i\mathbf{G}_m\cdot\mathbf{r}} \quad (5.27)$$

where  $\mathbf{G}_m$  is a reciprocal lattice vector. The one-particle wave function can now be written

$$\psi_{\mathbf{k}}(\mathbf{r}) = \left( \sum_m c_{\mathbf{k},m} e^{i\mathbf{G}_m\cdot\mathbf{r}} \right) e^{i\mathbf{k}\cdot\mathbf{r}} = \sum_m c_{\mathbf{k},m} e^{i(\mathbf{k}+\mathbf{G}_m)\cdot\mathbf{r}} \quad (5.28)$$

If the effective potential is local it can also be expanded in a similar way

$$v_{\text{eff}}(\mathbf{r}) = \sum_m v_{\text{eff}}(\mathbf{G}_m) e^{i\mathbf{G}_m\cdot\mathbf{r}} \quad (5.29)$$

Substituting these expressions back into the Kohn-Sham Equation (5.19),

$$\left(-\frac{1}{2}\nabla^2 + v_{\text{eff}}(\mathbf{r})\right)\psi_{\mathbf{k}}(\mathbf{r}) = \varepsilon_{\mathbf{k}}\psi_{\mathbf{k}}(\mathbf{r}) \quad (5.30)$$

a reciprocal space equation for the coefficients  $c_{\mathbf{k},m}$  can be obtained as

$$\frac{1}{2}|\mathbf{k} + \mathbf{G}_m|^2 c_{\mathbf{k},m} + \sum_{m'} v_{\text{eff}}(\mathbf{G}_m - \mathbf{G}_{m'}) c_{\mathbf{k},m} = \varepsilon_{\mathbf{k}} c_{\mathbf{k},m} \quad (5.31)$$

The original Kohn-Sham differential equation has now been rewritten as a matrix equation, one for each value of  $\mathbf{k}$ , where the matrix Hamiltonian is

$$H_{m,m'}(\mathbf{k}) = \frac{1}{2}|\mathbf{k} + \mathbf{G}_m|^2 \delta_{m,m'} + v_{\text{eff}}(\mathbf{G}_m - \mathbf{G}_{m'}) \quad (5.32)$$

The problems are that there are infinitely many  $\mathbf{k}$ -points to consider and that the Hamiltonian matrix in principle is of infinite dimension. In practise both these infinities can be handled by considering only a finite number of  $\mathbf{k}$ -points and reciprocal lattice vectors  $\mathbf{G}$ .

### 5.7.2 Finite sampling

It follows from Bloch's theorem (Equation (5.26)) that if  $\psi_{\mathbf{k}}$  is a solution, then so is  $\psi_{\mathbf{k}+\mathbf{G}}$ . The solutions can therefore be restricted to the primitive reciprocal unit cell, called the Brillouin zone. However, there is still an uncountably infinite number of  $\mathbf{k}$ -points to consider. This is handled through discrete sampling of the Brillouin zone. In this thesis the common method of Monkhorst and Pack [97] has been used. The method selects  $N_i$   $\mathbf{k}$ -points along each reciprocal lattice vector  $\mathbf{b}$  according to the scheme

$$u_{n_i} = \frac{2n_i - N_i - 1}{2N_i} \quad n_i \in [1, N_i] \quad (5.33)$$

$$\mathbf{k}_{n_1, n_2, n_3} = u_{n_1}^{(1)} \mathbf{b}_1 + u_{n_2}^{(2)} \mathbf{b}_2 + u_{n_3}^{(3)} \mathbf{b}_3 \quad (5.34)$$

Due to symmetry in the crystal this can be reduced even further, to the irreducible Brillouin zone, and in practise, especially for crystals of high symmetry, only a few  $\mathbf{k}$ -points will suffice to determine the electron density in the entire crystal.

The infinite sum over  $m'$  and thus the dimension of the Hamiltonian matrix can be truncated at a cut-off energy  $\frac{1}{2}|\mathbf{k} + \mathbf{G}|^2 < E_{\text{cut}}$ . This introduces a small error and  $E_{\text{cut}}$  has to be chosen judiciously taking both accuracy and computational cost into account. Usually, the energy cut-off is taken as a value beyond which accuracy increases only marginally when increasing the cut-off energy. The exact value of  $E_{\text{cut}}$  will depend on how the core electrons are treated. By using the pseudopotential method  $E_{\text{cut}}$  can be reduced greatly.

### 5.7.3 Pseudopotentials and PAW

A problem with plane wave basis sets is that rapidly varying functions, such as the wave functions close to heavy nuclei, require a very high cut-off energy in order to be well represented. One solution to this is the *pseudopotential* method in which the potential in the core region, i.e. the nucleus and the innermost electrons, are replaced by a different potential [98]. The argument for this is that the core electrons do not take part in and are to a large degree unaffected by chemical bonding. Among the requirements on pseudopotentials are that they should reproduce the true potential and electron density of the all-electron problem outside the core region as well as energy eigenvalues and be smooth enough that a low  $E_{\text{cut}}$  is possible.

Although the pseudopotentials are smoother than the original all-electron potentials they can be made even smoother by relaxing the norm-conserving condition. A norm-conserving pseudopotential generates pseudo wavefunctions which obey the usual orthogonality relation of wavefunctions. By relaxing the norm-conserving constraint it is possible to formulate ultrasoft pseudopotentials [99, 100], which reach the goal of accuracy while being much smoother and thus requiring decidedly smaller cut-off energy.

The ultrasoft pseudopotential method was given a firm theoretical footing by the works of Blöchl [101] and Kresse and Joubert [102] in the *Projector Augmented Wave* (PAW) method. The PAW method prescribes a linear mapping  $\mathcal{T}$  which projects the pseudo wavefunctions inside the core regions onto the true all-electron wave functions. The PAW is therefore effectively an all-electron method giving access to the core electron states while still preserving all the benefits of a plane wave pseudopotential. In practise however, the frozen-core approximation is usually applied, in which the core states are not updated. This approximation usually leads to sufficient accuracy [103].

## Vibrational motion

With the electronic structure problem formally solved it is time to turn to the vibrational motion of the ions. As discussed in Section 3.3 the free energy for the vibrational motion can be rather easily obtained if just the vibrational frequencies are known. The frequencies can be obtained by diagonalising the ionic Hamiltonian in Equation (5.6), which is obtained after applying the adiabatic approximation.

Although it is possible to write down a formal expression for the potential  $V(\mathbf{R})$  in Equation (5.6), it is customary to expand the potential in a Taylor series. In the *harmonic approximation* the potential is expanded to second order. The second order term is a matrix, which can be computed using first principle methods, and can be diagonalised to yield the eigenmodes and eigenfrequencies for the vibrational motion. These eigenmodes are collective lattice vibrations called *phonons* which oscillate in a harmonic potential for which the quantum mechanical solutions are known.

It is instructive to start the discussion about lattice vibrations with a one dimensional diatomic chain as many of the conclusions can be carried over to the three dimensional case while at the same time being more transparent [66, 69].

### 6.1 One-dimensional diatomic chain

Assume a periodic chain of atoms of types A and B, with masses  $M_1$  and  $M_2$  separated a distance  $a/2$ , where  $a$  is the period of the chain, and connected with springs with spring constant  $c$  (see Figure 6.1). Denote the deviation from the equilibrium position by  $u_n$  and  $v_n$  for the atoms A and B respectively in unit cell  $n$ . By Hooke's law the atom A in unit cell  $n$  will then experience a restoring force equal to  $F = c(v_n - u_n) + c(v_{n-1} - u_n) = (-2u_n + v_{n-1} + v_n)c$ , and analogously

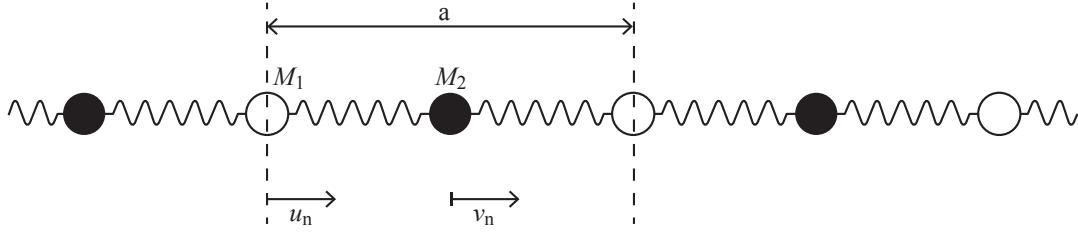


Figure 6.1: One-dimensional diatomic chain

for atom type B. By applying Newton's second law for both atom types we get two coupled differential equations

$$\begin{cases} M_1 \ddot{u}_n = (-2u_n + v_{n-1} + v_n)c \\ M_2 \ddot{v}_n = (-2v_n + u_n + u_{n+1})c \end{cases} \quad (6.1)$$

The right hand side of Equation (6.1) is the one dimensional equivalent of what will later be called the Force Constant (FC) matrix, times the displacement vector. A general form of solution to a second order differential equation is

$$u_n(t) = \frac{1}{\sqrt{M_1}} \tilde{u}_n e^{-i\omega t}; \quad v_n(t) = \frac{1}{\sqrt{M_2}} \tilde{v}_n e^{-i\omega t} \quad (6.2)$$

which reduces the Equation (6.1) to

$$\begin{cases} -\omega^2 \tilde{u}_n = -\frac{2c}{M_1} \tilde{u}_n + \frac{c}{\sqrt{M_1 M_2}} \tilde{v}_{n-1} + \frac{c}{\sqrt{M_1 M_2}} \tilde{v}_n \\ -\omega^2 \tilde{v}_n = -\frac{2c}{M_2} \tilde{v}_n + \frac{c}{\sqrt{M_1 M_2}} \tilde{u}_n + \frac{c}{\sqrt{M_1 M_2}} \tilde{u}_{n+1} \end{cases} \quad (6.3)$$

By assuming plane wave like solutions we can introduce a phase factor dependence

$$\tilde{u}_n = U e^{iqx_n}; \quad \tilde{v}_n = V e^{iqx_n} \quad (6.4)$$

where  $x_n$  is the position of the atoms in unit cell  $n$ . This can be written as  $x_n = na$  and  $x_n = (n+1/2)a$  for atoms A and B respectively. Equation (6.1) is now reduced to

$$\begin{cases} -\omega^2 U = -\frac{2c}{M_1} U + \frac{c}{\sqrt{M_1 M_2}} e^{+iqa/2} V + \frac{c}{\sqrt{M_1 M_2}} e^{-iqa/2} V \\ -\omega^2 V = -\frac{2c}{M_2} V + \frac{c}{\sqrt{M_1 M_2}} e^{+iqa/2} U + \frac{c}{\sqrt{M_1 M_2}} e^{-iqa/2} U \end{cases} \quad (6.5)$$

This can now be written as an eigenvalue problem in matrix notation

$$\omega_{q\pm}^2 \mathbf{e}_{q\pm} = \mathbf{D}(q) \mathbf{e}_{q\pm} \quad (6.6)$$

Here  $\mathbf{e}_{q\pm} = (U_{\pm}, V_{\pm})^{\top}$  are the eigenvectors and

$$\mathbf{D}(q) = \begin{bmatrix} \frac{2c}{M_1} & -\frac{2c}{\sqrt{M_1 M_2}} \cos\left(\frac{qa}{2}\right) \\ -\frac{2c}{\sqrt{M_1 M_2}} \cos\left(\frac{qa}{2}\right) & \frac{2c}{M_2} \end{bmatrix} \quad (6.7)$$

is called the *Dynamical matrix*. This eigenvalue problem can now be solved to yield the eigenfrequencies and eigenmodes of the vibration. As with any  $2 \times 2$  matrix there are two solutions

$$\omega_{\pm}^2 = \frac{c}{M_1 M_2} \left[ (M_1 + M_2) \pm \sqrt{(M_1 + M_2)^2 - 4M_1 M_2 \sin^2\left(\frac{qa}{2}\right)} \right] \quad (6.8)$$

In this case the solutions are non-degenerate and non-negative. The solutions are illustrated in Figure 6.2 as functions of  $q$ . It is already apparent, due to the periodicity of the cosine function, that the only region of interest is the first Brillouin zone, i.e. when  $|q| \leq \frac{\pi}{a}$ . The formal expression for the eigenvector  $\mathbf{e}_{\pm} = (U_{\pm}, V_{\pm})^{\top}$  is

$$\frac{U_{\pm}}{V_{\pm}} = \frac{c(1 + e^{-iqa})}{2c - \omega_{\pm}^2 M_1} \quad (6.9)$$

It should be stressed that no assumption has yet been made as to the direction of the displacements  $u_n$  and  $v_n$ . If the displacement is along the direction of propagation the mode is called *longitudinal*. The two perpendicular modes are called *transversal*. The different modes will in general have different coupling constants  $c$  in Equation (6.6).

### 6.1.1 High symmetry points

Two limiting cases are of particular interest, the limits when  $qa \rightarrow 0$  and when  $qa \rightarrow \pi$ . The first case, the zone centre where  $q = 0$  is called the  $\Gamma$ -point. This is true also in higher dimensions. The solutions near the  $\Gamma$ -point are

$$\omega_{\Gamma}^2 = 2c \left( \frac{1}{M_1} + \frac{1}{M_2} \right) \quad (\text{optical mode}) \quad (6.10)$$

$$\omega_{\Gamma}^2 = \frac{1}{2} \frac{c}{M_1 + M_2} q^2 a^2 \quad (\text{acoustic mode}) \quad (6.11)$$

We note immediately that there are two distinct types of solutions to Equation (6.6), one optic and one acoustic mode separated by a bandgap. The eigenvector (Equation (6.9)) for the optical mode is reduced to

$$\frac{U}{V} = -\frac{M_2}{M_1} \quad (6.12)$$

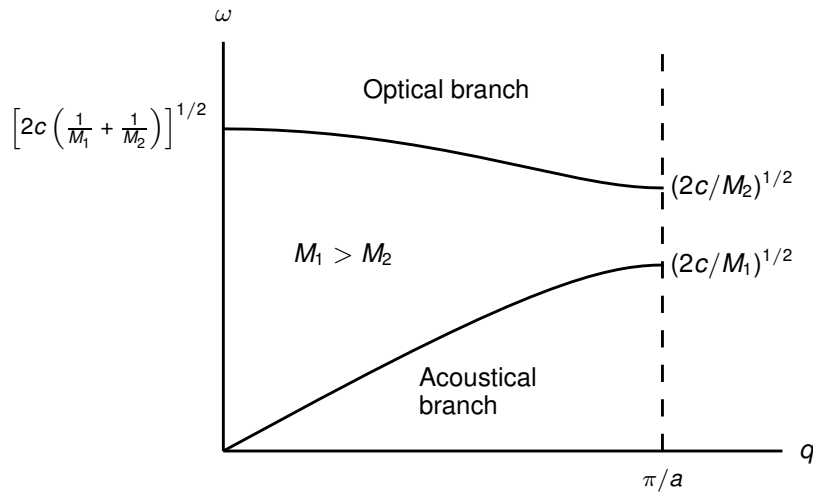


Figure 6.2: One-dimensional diatomic chain dispersion relation

which shows that, at the  $\Gamma$  point, the atoms vibrate against one another with the centre of mass fixed. For the acoustic mode, the ratio is 1 and the atoms vibrate in phase and with the same amplitude. This infinite wavelength limit is equivalent to a pure translation of the lattice.

The zone boundary, where  $q = \pi/a$  is another special or high symmetry point. The points have different designations in different symmetries. In 1D, the zone boundary point usually isn't given a name, but for convenience it will henceforth be denoted X in analogy with the point (1,0,0) in a 3D simple cubic lattice (see Figure 2.1b). The eigenfrequencies at the zone boundary are

$$\omega_X^2 = \frac{2c}{M_2} \quad (\text{optical mode}) \quad (6.13)$$

$$\omega_X^2 = \frac{2c}{M_1} \quad (\text{acoustic mode}) \quad (6.14)$$

The eigenvectors become  $\mathbf{e}_+ = (0, 1)$  and  $\mathbf{e}_- = (1, 0)$  for the optical and acoustic modes respectively. This means that in the optic mode only the lighter atoms move and in the acoustic only the heavier.

Since the displacement of atom A in unit cell  $n$  is

$$u_n = \frac{1}{\sqrt{M_1}} U e^{i(qan - \omega t)} \quad (6.15)$$

we can express the displacement of the atom in the neighbouring unit cell as

$$\begin{aligned}
 u_{n+1} &= \frac{1}{\sqrt{M_1}} U e^{i(qa(n+1) - \omega t)} \\
 &= \frac{1}{\sqrt{M_1}} U e^{iqa} e^{i(qan - \omega t)} \\
 &= u_n e^{iqa}
 \end{aligned} \tag{6.16}$$

and analogously for the B atom. Thus, at the  $\Gamma$ -point where  $q = 0$  all atoms of the same type move in the same direction, while at the Brillouin zone boundary where  $q = \pi/a$  and  $e^{iqa} = -1$  the atoms in neighbouring unitcells move in opposite directions.

### 6.1.2 Limiting cases I. Identical masses

The bandgap between the two branches at the zone boundary depends on the difference between the masses. In the limiting case when the masses  $M_1 = M_2$  are equal the bandgap closes. This is because the atoms are now identical and the primitive unit cell is only half that of the unit cell in Figure 6.1. As a consequence the Brillouin zone is extended to  $\frac{2\pi}{a}$ . The point at  $q = \pi/a$  is no longer a zone boundary point and the two different branches are in fact only one branch. The points on the optical branch should be unfolded to the region between  $q = \pi/a$  and  $q = 2\pi/a$  such that the  $\Gamma$ -point ends up on  $q = 2\pi/a$ .

### 6.1.3 Limiting cases II. Localised vibrations

In the limit when  $M_2/M_1 \rightarrow 0$  the dispersion of the optical branch goes to zeros and the eigenfrequency becomes independent of  $q$ . The motion of one particular atom in one particular unit cell is thus independent of the motion of the atoms in neighbouring unit cells. The eigenvectors will, in this limit, become the same at the  $\Gamma$  point and at the zone boundary,  $\mathbf{e}_+ = (0, 1)$ . Thus the amplitude of the heavier atom will be negligible in comparison and the motion of the lighter is independent of  $q$ -value. In other words, the motion of one light atom is independent of the motion of any other atom in the lattice. Such a mode is called *localised*. The unit cell can be treated as if it were an isolated molecule with no periodicity. In this case only the  $\Gamma$  point has to be considered.

### 6.1.4 Application in oxyhydrides

The one-dimensional diatomic chain is used qualitatively in the study of the oxyhydride  $\text{BaTiO}_3$  in **Paper II**. The hydrogen vibrational modes are very localised

and it is possible to treat all ions as immobile, except for the oxygen and hydrogen ions along the O-Ti-H-Ti chain, with the hydrogen ion the lighter with mass  $M_2$  and the oxygen ion the heavier with mass  $M_1$ . The oxyhydride barium titanate is illustrated in Figure 2.4. In the mode of higher frequency the displacements are along the chain in a longitudinal manner and in mode of lower frequency the mode is two fold degenerate and perpendicular to the direction of the chain in a transverse manner. These three modes are seen as optical modes with very little dispersion in Figure 6.3. The effective mass for oxygen in atomic mass units is 83 for the longitudinal mode and 426 for the transverse modes, in both cases much larger than 16, the atomic mass for oxygen, which shows that the approximation of a one-dimensional diatomic chain in the limit of infinite mass for one of the atoms holds.

## 6.2 Phonons as lattice modes

In reality the atomic motion in a solid occur in three dimensions and the above model, albeit instructive and intuitive, needs to be generalised [66, 69–71].

The potential energy in a periodic solid,  $V(\mathbf{R})$ , is a function of the positions  $\mathbf{R}$  of all atoms in the crystal. Under the assumptions that the deviations from equilibrium are small the potential energy can be written as an expansion with respect to the displacements  $dR_{ni\alpha}$ . Furthermore, a local minimum is characterised by the first derivative being zero. By keeping only second order terms in what is called the harmonic approximation the potential can be written

$$V(\{\mathbf{R}\}) = V(\{\mathbf{R}_0\}) + \frac{1}{2} \sum_{ni\alpha, mj\beta} \frac{\partial^2 V(\{\mathbf{R}_0\})}{\partial R_{ni\alpha} \partial R_{mj\beta}} dR_{ni\alpha} dR_{mj\beta} \quad (6.17)$$

where  $V(\{\mathbf{R}_0\}) = E_0$  is the equilibrium energy and is a function of the equilibrium positions  $\{\mathbf{R}_0\}$  of all atoms. This is just an additive constant and we will choose the energy scale in the following such that  $E_0 = 0$ . The indices  $i, j$  indicate sum over atoms in the unit cell,  $n, m$  indicate sum over unit cells and  $\alpha, \beta$  the sum over cartesian directions.

With the notation for the displacements  $u = dR$  the nuclear Hamiltonian from Equation (5.6) can now be written (in the adiabatic approximation)

$$H_n = \sum_{ni\alpha} \frac{p_{ni\alpha}^2}{2M_i} + \frac{1}{2} \sum_{ni\alpha, mj\beta} F_{ni\alpha, mj\beta} u_{ni\alpha} u_{mj\beta} \quad (6.18)$$

The matrix  $F_{ni\alpha, mj\beta}$  is called the *Force Constant (FC) Matrix*. Due to the commutativity of the derivatives it is immediately obvious that the FC-matrix is

symmetric. The equations of motion become

$$M_i \ddot{u}_{ni\alpha} = - \sum_{mj\beta} F_{ni\alpha,mj\beta} u_{mj\beta} \quad (6.19)$$

By assuming wavelike solutions a general form of solution is of the form

$$u_{ni\alpha}(t) = \frac{1}{\sqrt{M_i}} \tilde{u}_{ni\alpha} e^{-i\omega t} \quad (6.20)$$

Inserting this Equation (6.19) can be written

$$\omega^2 \tilde{u}_{ni\alpha} = \sum_{mj\beta} \frac{1}{\sqrt{M_i M_j}} F_{ni\alpha,mj\beta} \tilde{u}_{mj\beta} \quad (6.21)$$

Let us now introduce a new matrix, which is a real space representation of the dynamical matrix<sup>1</sup>

$$\tilde{D}_{ni\alpha,mj\beta} = \frac{1}{\sqrt{M_i M_j}} F_{ni\alpha,mj\beta} \quad (6.22)$$

and has the dimension  $3 \times N \times M$ , where  $N$  is the number of atoms in the unit cell,  $M$  is the number of unit cells in the system and 3 is the dimensionality of the three dimensional space.

### 6.2.1 $q$ -space

In an (infinite) periodic solid it is convenient to introduce the  $q$ -space<sup>2</sup> representation, the *Dynamical Matrix*. Since the energy cannot depend on the absolute positions of cells  $n$  and  $m$ , only on their relative position  $\mathbf{R} = \mathbf{R}_n - \mathbf{R}_m$  we have

$$\tilde{D}_{ni\alpha,mj\beta} = \frac{1}{\sqrt{M_i M_j}} F_{ni\alpha,mj\beta} = \tilde{D}_{i\alpha,j\beta}(\mathbf{R}_n - \mathbf{R}_m) \quad (6.23)$$

By virtue of Bloch's theorem we can set the  $\mathbf{R}$ -dependence as a phase and write

$$\tilde{u}_{ni\alpha} = e_{i\alpha} e^{i\mathbf{q} \cdot \mathbf{R}_n} \quad (6.24)$$

which gives the eigenvalue problem as

$$\omega^2 e_{i\alpha} = \sum_{mj\beta} \tilde{D}_{i\alpha,j\beta}(\mathbf{R}_n - \mathbf{R}_m) e^{-i\mathbf{q} \cdot (\mathbf{R}_n - \mathbf{R}_m)} e_{j\beta} \quad (6.25)$$

<sup>1</sup>The literature is not completely consistent in the notation. Sometimes the FC-matrix is defined weighted with the masses, what is here called the real space dynamical matrix (cf. Equation 6.22), sometimes the opposite. Another name for the FC-matrix is the *Hessian matrix*

<sup>2</sup>The reciprocal space is customarily called  $k$ -space, but we will here use the notation  $q$ -space for the phonon motion in order not to confuse it with the electronic structure  $k$ -space.

With the definition

$$D_{i\alpha,j\beta}(\mathbf{q}) = \sum_{\mathbf{R}} \tilde{D}_{i\alpha,j\beta}(\mathbf{R}) e^{-i\mathbf{q}\cdot\mathbf{R}} = \sum_n e^{-i\mathbf{q}\cdot\mathbf{R}_n} \frac{1}{\sqrt{M_i M_j}} \frac{\partial^2 V}{\partial u_{ni\alpha} \partial u_{0j\beta}} \quad (6.26)$$

we now get the eigenvalue problem

$$\omega^2 e_{i\alpha} = \sum_{j,\beta} D_{i\alpha,j\beta}(\mathbf{q}) e_{j\beta} \quad (6.27)$$

or in matrix notation

$$\omega_{\mathbf{q}s}^2 \mathbf{e}_{\mathbf{q}s} = \mathbf{D}(\mathbf{q}) \mathbf{e}_{\mathbf{q}s} \quad (6.28)$$

where the index  $s$  denotes the  $3 \times N$  solutions at each  $\mathbf{q}$ -point. The original problem of diagonalising a  $3 \times N \times M$  matrix (where  $M$  in principle is infinite) has now been reduced to diagonalising  $K$  matrices (one for each value of  $\mathbf{q}$ ) of size  $3 \times N$ .

## 6.2.2 Atomic displacements

Once the eigenvectors are found the displacement of ion  $i$  at lattice vector  $\mathbf{R}_n$  will be given by

$$\mathbf{u}_{nis}(\mathbf{q}, t) = \frac{1}{\sqrt{M_i}} \mathbf{e}_{i\mathbf{q}s} e^{i(\mathbf{q}\cdot\mathbf{R}_n - \omega_{\mathbf{q}s} t)} \quad (6.29)$$

where  $\mathbf{e}_{i\mathbf{q}s}$  is the set of  $d$  components of the eigenvector solutions to Equation (6.28) that denote the displacement of ion  $i$  at frequency  $\omega_{\mathbf{q}s}$  in  $d$  dimensions. The full eigenmode of a particular frequency  $\omega_{\mathbf{q}s}$  is given by the sum over  $i$ . The most general displacement of ions is the superposition of all linearly independent elementary solutions and can be written as

$$\mathbf{u}_{ni}(t) = \frac{1}{\sqrt{M_i}} \sum_{s,\mathbf{q}} (c_{s\mathbf{q}} \mathbf{e}_{i\mathbf{q}s} e^{i\mathbf{q}\cdot\mathbf{R}_n} e^{i\omega t} + c_{s\mathbf{q}}^* \mathbf{e}_{i\mathbf{q}s}^* e^{-i\mathbf{q}\cdot\mathbf{R}_n} e^{-i\omega t}) \quad (6.30)$$

where the arbitrary (complex) constants  $c_{s\mathbf{q}}$  are the analogue to the amplitude.

By writing  $Q_{s\mathbf{q}}(t) = \sqrt{N} (c_{s\mathbf{q}} e^{i\omega_{\mathbf{q}s} t} + c_{s\mathbf{q}}^* e^{-i\omega_{\mathbf{q}s} t})$  it is possible to show [69, 70] that the ionic Hamiltonian in (6.18) can be written as

$$H = \frac{1}{2} \sum_{\mathbf{q}s} P_{\mathbf{q}s} P_{\mathbf{q}s}^* + \omega_{\mathbf{q}s}^2 Q_{\mathbf{q}s} Q_{\mathbf{q}s}^* \quad (6.31)$$

where  $P_{\mathbf{q}s}(t) = \dot{Q}_{\mathbf{q}s}(t)$  and the asterisk denotes the hermitian conjugate. This formally diagonalises the Hamiltonian and is identical to a set of independent harmonic oscillators with frequencies  $\omega_{\mathbf{q}s}$ , where  $Q_{\mathbf{q}s}$  and  $P_{\mathbf{q}s}$  are the generalised positions and momenta respectively of collective motions. Each vibrational mode

can be represented as a quantum mechanical quasi-particle called phonon. We can now write the vibrational free energy calculated in Section 3.3 for a periodic solid as

$$F_{\text{vib}} = \sum_{\mathbf{q}s} \left( \frac{\hbar\omega_{\mathbf{q}s}}{2} + k_B T \ln(1 - e^{-\beta\hbar\omega_{\mathbf{q}s}}) \right) = E_0 + k_B T \sum_{\mathbf{q}s} \ln(1 - e^{-\beta\hbar\omega_{\mathbf{q}s}}) \quad (6.32)$$

where  $E_0$  is the zero point energy.

### 6.2.3 Bandspectrum

The vibrational properties of a periodic system are given by its eigenfrequencies, found by diagonalising the Dynamical matrix at each respective  $q$ -point in the first Brillouin zone. However, illustrating this in a figure is not as straight forward as in the one-dimensional case in Figure 6.2 since  $\mathbf{q}$  is a three-dimensional vector. It is therefore necessary to plot the vibrational frequencies only at selected points of high symmetry in the Brillouin zone and along the path that connects them in a *bandspectrum*. As an example of a bandspectrum Figure 6.3 shows the bandspectra of pristine cubic BaTiO<sub>3</sub> and SrTiO<sub>3</sub> along the high symmetry paths illustrated in Figure 2.1b as well as the bandspectrum of the oxyhydride BaTiO<sub>3-x</sub>H<sub>x</sub> in a 40 atom simulation cell.

### 6.2.4 Density of State

Often, it is not necessary to illustrate the full vibrational spectrum. Rather, it is sufficient or even desirable to present only a the *density of state* (DOS).

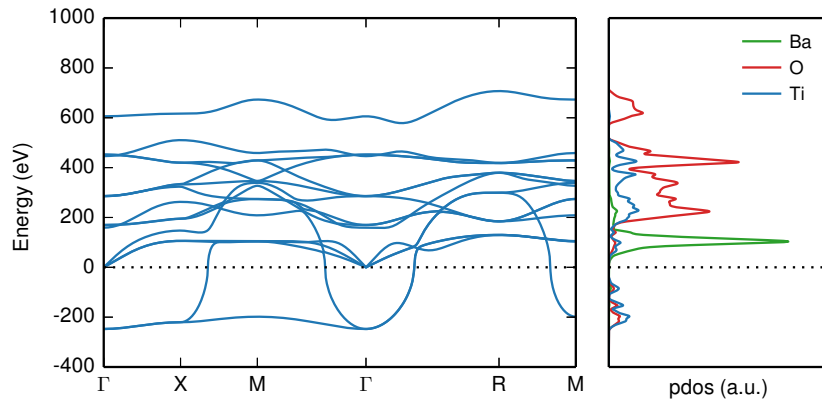
The density of state is a convenient measure of the number of phonons in the interval  $[\omega, \omega + d\omega]$  independent of the  $\mathbf{q}$ -vector. Formally this can be written as

$$g(\omega) = \sum_{s\mathbf{q}} \delta(\omega - \omega_{\mathbf{q}s}) \quad (6.33)$$

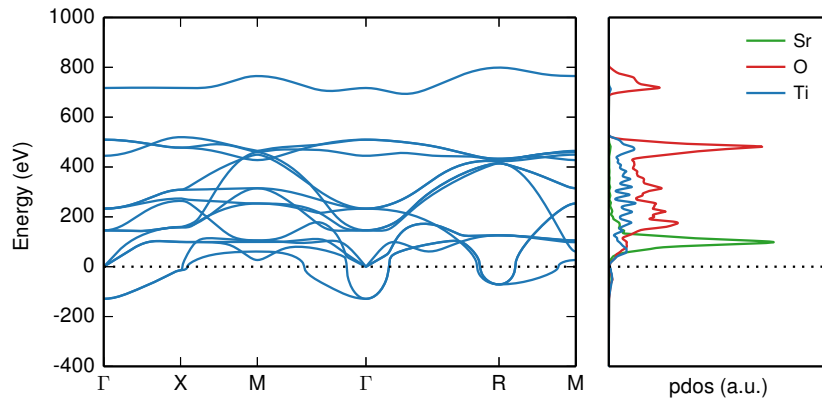
By integrating the DOS

$$n(\omega) = \int_0^\omega g(\omega') d\omega' \quad (6.34)$$

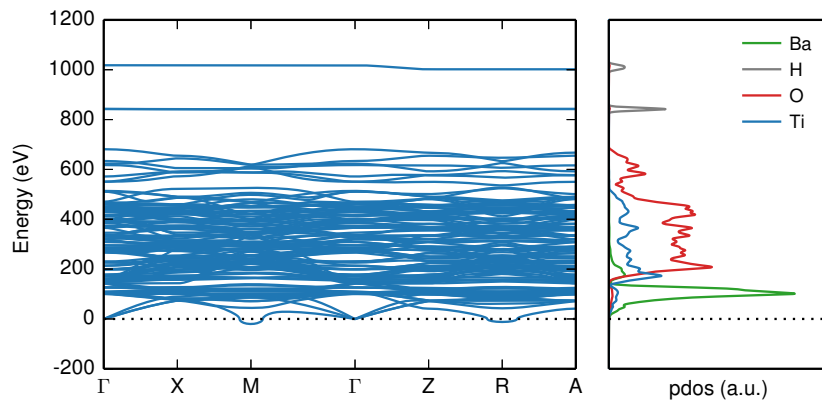
the number of modes with frequencies below or equal to  $\omega$  is obtained. By integrating over all frequencies the total number of  $3N$  modes is obtained, where  $N$  is the number of atoms in the unit cell.



(a) BTO



(b) STO



(c) BaTiO<sub>3-x</sub>H<sub>x</sub>

Figure 6.3: Illustration the bandspectrum (left) and PDOS (right) of (a) pristine cubic BaTiO<sub>3</sub> (top), (b) pristine cubic SrTiO<sub>3</sub> (middle) and (c) oxyhydride BaTiO<sub>3-x</sub>H<sub>x</sub> (bottom).

The DOS is useful in the thermodynamic limit of an infinite crystal where the sum over  $\mathbf{q}$  in e.g. Equation (6.32) approaches an integral. Using the identity

$$\sum_{s\mathbf{q}} f(\mathbf{q}) = \sum_s \frac{\Omega_c}{(2\pi)^3} \int_{BZ} d\mathbf{q} f(\mathbf{q}) = \int D(\omega) f(\omega) d\omega \quad (6.35)$$

where  $\Omega_c$  is the volume of the unit cell, the free energy can be written as

$$\begin{aligned} F_{\text{vib}} &= \sum_{s\mathbf{q}} \left( \frac{\hbar\omega_{\mathbf{q}s}}{2} + k_B T \ln(1 - e^{-\beta\hbar\omega_{\mathbf{q}s}}) \right) \\ &= \sum_s \frac{\Omega_c}{(2\pi)^3} \int_{BZ} d\mathbf{q} \left( \frac{\hbar\omega_{\mathbf{q}s}}{2} + k_B T \ln(1 - e^{-\beta\hbar\omega_{\mathbf{q}s}}) \right) \\ &= \int D(\omega) \left( \frac{\hbar\omega}{2} + k_B T \ln(1 - e^{-\beta\hbar\omega}) \right) d\omega \end{aligned} \quad (6.36)$$

In computer simulations it is possible to separate the contribution from different elements. The *partial density of states* (PDOS) is the density of state caused by the motion of atom  $i$

$$d_i(\omega) = \sum_{s\mathbf{q}} |\mathbf{e}_{i\mathbf{q}s}|^2 \delta(\omega - \omega_{\mathbf{q}s}) \quad (6.37)$$

If the atom  $i$  does not participate in the mode at frequency  $\omega_{\mathbf{q}s}$ , the corresponding eigenvector  $\mathbf{e}_{i\mathbf{q}s}$  will be the zero vector and the partial density of state at this frequency is zero. As an example Figure 6.3 shows the PDOS of pristine cubic BaTiO<sub>3</sub> and SrTiO<sub>3</sub> as well as the PDOS of the oxyhydride BaTiO<sub>3-x</sub>H<sub>x</sub> in a 40 atom simulation cell. The correspondence between the bandspectrum and density of state is clearly seen.

In e.g. a neutron scattering experiment it is not the eigenvector that is measured but the displacement of the atoms in a vibrational mode. The displacement is inversely proportional to the square root of the masses (cf. Equation (6.29)) and lighter atoms will cause a stronger signal. Therefore, it is sometime appropriate to present the mass weighted projected density of state

$$w_i(\omega) = \frac{1}{M_i} d_i(\omega) = \frac{1}{M_i} \sum_{s\mathbf{q}} |\mathbf{e}_{i\mathbf{q}s}|^2 \delta(\omega - \omega_{\mathbf{q}s}) = \sum_{s\mathbf{q}} |\mathbf{u}_{nis}(\mathbf{q})|^2 \delta(\omega - \omega_{\mathbf{q}s}) \quad (6.38)$$

### 6.2.5 Limiting case. Localised modes.

Despite the collective nature of phonons, there are cases where only a few atoms take part in a certain mode. These modes are called local or localised modes [104]. Localised modes were discussed briefly in Section 6.1.3 in the special case for the one-dimensional diatomic chain. A localised mode is a phonon mode concentrated

in a region of space and in which only a few atoms participate in the vibration while the rest of the lattice remains at rest. The eigenvector for such a mode will be non-zero only for a few elements which typically are much lighter than all the others and will to a good approximation form a sub-matrix in a block diagonal dynamical matrix. The dynamical matrix in Equation (6.26) can thus be obtained as a limiting case of  $M_j \rightarrow \infty$  for all  $j \neq i$ , where  $i$  is the lighter atom. If a mode is local most elements in will be zero and the dynamical matrix  $D_{i\alpha,j\beta}(\mathbf{q})$  will span a relatively small space.

A local mode is typically also rather  $\mathbf{q}$ -point independent, and there is no need to go to reciprocal space. The vibrational mode is well enough represented at the  $\Gamma$ -point by the Force Constant matrix  $F_{ni\alpha,mj\beta}$ . By the argument above only a part of the FC-matrix needs to be computed in order to describe the vibrational mode [104, 105].

One such local mode is the hydrogen mode in  $\text{BaTiO}_{3-x}\text{H}_x$  which is shown in Figure 6.3c. A  $3 \times 3$  Force Constant sub-matrix can be constructed by displacing only the hydrogen ion in three directions. By diagonalising only the non-zero sub-matrix the hydrogen vibrational frequencies and eigenmodes can be obtained.

## 6.2.6 Lattice stability

Although the dynamical matrix is Hermitian and as a consequence has only real eigenvalues, there is nothing preventing the existence of negative eigenvalues. Since the eigenvalue is the square of the frequency the existence of imaginary frequencies has to be addressed.

Assume that there is an eigenvalue  $\omega_{\mathbf{q}s}^2 = -\gamma < 0$ . Then  $\omega = i\sqrt{\gamma}$  will be a purely imaginary number and the displacement (cf. Equations (6.15) and (6.29)) will behave as  $e^{\pm\gamma t}$ . Any disturbance will grow exponentially and the crystal is not stable. This corresponds to a negative spring constant  $c$  in the one dimensional case. The force is not restoring but repelling and the larger the displacement the larger the repelling force.

Since it is a requirement that all vibrational frequencies be positive it is thus the formal criterion of lattice stability is that the matrix of second order derivatives, the Hessian matrix, is positive definite. The presence of imaginary modes indicate that the investigated structure at  $\{\mathbf{R}_0\}$ , although at a stationary point as assumed in Equation (6.17), is not at an energy minimum but at a saddle point [106]. The imaginary frequencies indicate that a lower energy structure can be found by displacing the atoms in the crystal along the eigenvector associated with the imaginary frequency.

One example of a lattice instability is mentioned in **Paper II**. Barium titanate in its high temperature phase is cubic perovskite. However, in a phonon calculation  $\text{BaTiO}_3$  exhibits imaginary modes. This indicates that cubic  $\text{BaTiO}_3$  is not stable

at 0 K, and experimentally there is indeed a phase transition away from cubic perovskite already at 120°C.

Since the cubic phase is stable at some temperature it should in principle be possible to stabilize the crystal by minimising not the energy but the *free energy* at the relevant temperature. By computing the vibrational entropy, and the free energy, at various lattice constants it is possible to obtain the free energy potential instead of only the internal energy. The technique is commonly referred to as the quasi harmonic approximation [63, 64]. The quasi harmonic approximation is based on the assumption that the harmonic approximation holds at every value of the lattice constant, which is treated as an adjustable parameter. Within the quasi harmonic approximation it is possible to compute, among other things, the thermal lattice expansion, which is out of reach within the harmonic approximation. However, also the quasi harmonic approximation fails ultimately when the temperature increases and the displacements away from equilibrium become too large and higher order terms need to be included in the potential energy expansion in Equation (6.17) [107].

As an example, Figure 6.3 shows the bandspectra of pristine cubic BaTiO<sub>3</sub> and SrTiO<sub>3</sub> along the high symmetry points illustrated in Figure 2.1b. The phase transition of BTO mentioned in Section 2.3 above is clearly seen as imaginary frequencies (on the negative y-axis) at the  $\Gamma$ -point, but also along the entire paths connecting  $\Gamma$ ,  $M$  and  $X$ . STO also exhibits this imaginary frequency at the gamma point showing that STO also, in principle, could be prone to a ferroelectric transition [108]. However, in practise STO does not exhibit the ferroelectric phase transition of BTO [19] because of the  $R$ -mode instability which makes the TiO<sub>6</sub> octahedra in STO tilt into an anti-ferroelectric phase described in Section 2.3. BTO on the other hand is not prone to the anti-ferroelectric transitions of STO due to the lack of imaginary frequencies at the  $R$ -point.

## 6.3 Computational aspects

In order to solve the eigenvalue problem Equation (6.28) the quantity to be computed is the dynamical matrix, reprinted here for convenience.

$$D_{i\alpha,j\beta}(\mathbf{q}) = \sum_n e^{-i\mathbf{q}\cdot\mathbf{R}_n} \frac{1}{\sqrt{M_i M_j}} \frac{\partial^2 V}{\partial u_{ni\alpha} \partial u_{0j\beta}} \quad (6.26)$$

Even though the original problem of diagonalising a  $3 \times N \times M$  matrix (where  $M$  in principle is infinite) now has been reduced to diagonalising  $K$  matrices (one for each value of  $\mathbf{q}$ ) of size  $3 \times N$ , the calculation of the dynamical matrix in Equation (6.28) is still immense. If the crystal is infinite the number of  $\mathbf{q}$ -vectors is in principle also infinite. However, it turns out that a judiciously chosen finite

number of  $\mathbf{q}$ -points, e.g. using a Monkhorst-Pack [97] grid, works well enough. The symmetry of the lattice further reduces the number of  $\mathbf{q}$ -points at which a matrix has to be diagonalised to the irreducible Brillouin zone. The principle is the same as for the electronic structure in Section 5.7.2.

Not only are the number of  $\mathbf{q}$ -vectors infinite, in an infinite crystal the sum over unit cells,  $n$ , is also infinite. Fortunately acceptable accuracy can often be obtained with a finite number of unit cells  $n$ , i.e.  $\mathbf{R}_n$  is limited the period of a supercell of modest size.

In the present thesis the matrix elements are obtained using **phonopy** [64] which is a software implementation of the *frozen phonon* approach. In the frozen phonon approach the motion of the  $i$ :th atom is frozen in at a finite displacement  $\delta$  and the forces on each ion are calculated from the relaxed electronic structure. This works rather well if the displacements are small enough not to violate the harmonic approximation but large enough for numerical accuracy. The forces are typically given as the Hellmann-Feynman forces directly from an electronic structure calculation. The matrix elements can be computed using finite differentiation and central differences.

$$\begin{aligned}
 F_{ni\alpha,0j\beta} &= \frac{\partial^2 V(\mathbf{u})}{\partial u_{ni\alpha} \partial u_{0j\beta}} = \frac{\partial}{\partial u_{ni\alpha}} \left( \frac{\partial V(\mathbf{u})}{\partial u_{0j\beta}} \right) = -\frac{\partial f_{0j\beta}(\mathbf{u})}{\partial u_{ni\alpha}} \\
 &\approx -\frac{f_{0j\beta}(u_1, \dots, u_{ni\alpha} + \Delta, \dots, u_{3N}) - f_{0j\beta}(u_1, \dots, u_{ni\alpha} - \Delta, \dots, u_{3N})}{2\Delta}
 \end{aligned} \tag{6.39}$$

### 6.3.1 Localised hydrogen modes

In **Paper II** the localised hydrogen modes for  $\text{BaTiO}_{3-x}\text{H}_x$  were obtained in a slightly different, albeit mathematically equivalent, manner. Since the eigenmodes could be deduced *a priori* from symmetry arguments, there was no need for computing the mixed derivatives. In addition, since the mode is very local and contained only one atom any interaction between atoms could be neglected both within the unitcell (with indices  $i, j$ ) as well as between unitcells (with indices  $n, m$ ). To stress this independence these indices have been dropped below. The diagonal terms in the FC sub-matrix

$$F_{\alpha\alpha} = \frac{\partial^2 V}{\partial u_\alpha^2} \tag{6.40}$$

were computed by fitting second order polynomials of type  $\frac{1}{2}m\omega^2 x^2$ , where  $m$  is the mass of the atom,  $\omega$  the vibrational frequency and  $x$  the displacement away from the equilibrium position, to the energy landscape obtained by displacing the ions in both positive and negative directions along the eigenvectors as illustrated in

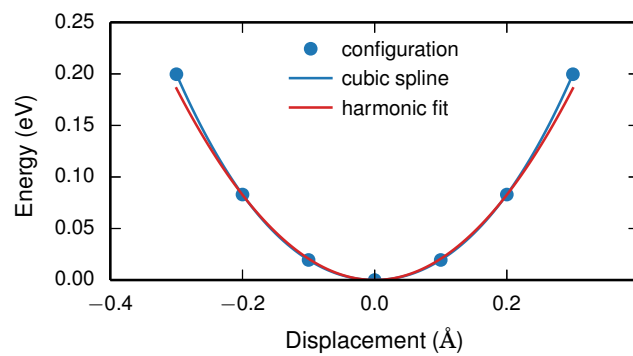


Figure 6.4: Illustration of potential well mapping

Figure 6.4. In **Paper II** the method is called the one particle harmonic potential (OPHP) method.



## Summary of appended articles

### 7.1 Paper I

In hydration of a solid state proton conductor the vacancies are filled with hydroxide ions according to the reaction



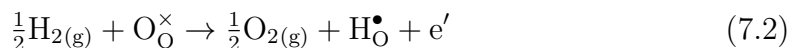
The hydrogen ion is rather loosely bound to the oxygen and is mobile as a positively charged proton. The difference in ionic radius between the hydroxide ion and the vacancy causes the material to expand during hydration. This volume difference is investigated in **Paper I** for  $\text{BaZrO}_3$ .

In **Paper I** we developed a strain tensor formalism which describes not only the size, i.e. the ionic radius, but also the anisotropy induced by the defect. The trace of the strain tensor is directly related to the volume of the defect from which an ionic radius can be obtained. The strain tensor is general and applicable to any point defect in any material describing not only the volume expansion but also the anisotropy.

The strain tensor formalism is also applied to the defects involved in hydration of  $\text{BaZrO}_3$  i.e. the proton and the oxygen vacancy, including some acceptor dopants necessary for the formation of the vacancies. We conclude that the vacancy is smaller than the oxygen host ion but more interestingly, also the hydroxide ion is smaller than the oxygen ion. The cause of the chemical expansion during hydration is not the large size of the proton, but the relatively small size of the vacancy.

## 7.2 Paper II

In **Paper II** we investigate the substitutional hydrogen  $\text{H}_\text{O}^\bullet$  which can form in  $\text{BaTiO}_3$  and consists of a negatively charged  $\text{H}^-$  ion on an oxygen site. It is formed from the reaction



and leads to  $n$ -type doping of the material. Doping into the initially empty Ti  $3d$  band should according to band theory lead to a delocalised electron. However, through coupling to phonons it can also lead to a polaron.

In order to localise an electron and form a polaron the DFT+ $U$  method is used and we determine the  $U$ -parameter self-consistently through applying the piecewise linearity constraint of the xc-functional. The exact value of the  $U$ -parameter is not transferable between different systems and we find that the  $U$ -value, and therefore also the lattice constant is different in a  $2 \times 2 \times 2$  supercell ( $U = 3.3$ ) and a  $3 \times 3 \times 3$  supercell ( $U = 3.1$ ). Polaron formation is found to be energetically favourable ( $\Delta E = -57$  meV) in the smaller supercell, but unfavourable ( $\Delta E = 124$  meV) in the larger indicating a concentration dependence for the polaron formation energy.

In order to determine the presence of polarons in oxyhydride BTO we note that the vibrational properties of the hydride ion changes significantly when a bound polaron is formed on the nearest neighbour titanium.

Because the HSE functional is known to produce more accurate vibrational frequencies, the frequencies are determined using the HSE xc-functional and the One Particle Potential method (also known as the Partial Hessian approach) which requires fewer displacements and consequently fewer calculations, only one displacement of the hydrogen atom in each of the three cartesian directions. This is possible due to the very localised nature of the hydrogen vibrations.

We discriminate between the two possible electronic states, the delocalised band-state and the localised polaron state, using inelastic neutron scattering. The agreement between the calculated vibrational frequencies and the measured spectrum leads to the conclusion that the conduction electrons in the measured sample are predominantly delocalised, although polarons also seem to be present when the concentration of hydride ions is increased, which is in agreement with the calculated polaron formation energies. Thereby, we also demonstrate that electronic defects can be characterised through vibrational properties by inelastic neutron scattering measurements.

## Summary and Outlook

In this thesis we have seen two examples of how first principles calculations can be used to penetrate a material, provide information about the local environment and how this affects macroscopic properties in a material.

In **Paper I** the chemical expansion, which is a difference in ionic volume between two different types of defects, could be separated into the formation volume of the two defects individually. Due to the charged nature of the defects this information is not easily accessible through experiments. The agreement between the measured and calculated chemical expansion suggests that the computational results are correct and that the chemical expansion can be understood from the separation into two individual effects. However, the agreement is not perfect and obviously there are effects, neglected in the article, which do have an influence, such as finite temperature and the quantum fluctuation of hydrogen.

In **Paper II** the oxyhydride barium titanate was investigated. The oxyhydride  $\text{BaTiO}_3$  is still a rather recent discovery and many aspects remain to be understood. For example whether yet further different types of hydrogen defects, such as substitutional dihydrogen, i.e. a hydrogen molecule or two hydrogen ions, on any type of site is possible, including the barium or titanium sites. Furthermore, pristine  $\text{BaTiO}_3$  is white whereas oxyhydride  $\text{BaTiO}_3$  is blue. There have been some attempts at explaining the blue colour, many of them including a bound polaron next to an oxygen defect such as the substitutional hydride or the oxygen vacancy, but a satisfactory explanation is yet to be provided. In addition, the elementary diffusion step, and thus the hydride exchange mechanism as well as the apparent thermodynamical instability needs further investigation.



# Acknowledgments

There are some people without whom this thesis could not have been written. Among these are my supervisor Göran Wahnström and co-supervisor Paul Erhart as well as my college Anders Lindman who has also co-authored both appended papers. I would also like to thank my collaborators Maths Karlsson and Carin Österberg who have contributed with experimental expertise and my research group at Materials and Surface Theory.

In addition I would like to thank people who have contributed with moral support throughout this work; Adam Arvidsson and Emil Ljungskog for all fruitful lunch discussions, my parents for all encouragement and my friends both at Chalmers and outside.

Finally I would like to thank my wife, Sofia, and my son, Alfred, for being my source of inspiration in life.



# Bibliography

- [1] K. Kreuer, *Proton-Conducting Oxides*, Annu. Rev. Mater. Res. **33**, 333 (2003).
- [2] R. H. Mitchell, *Perovskites: Modern and Ancient* (Almaz Press Thunder Bay, Thunder Bay, Ontario, Canada, 2002).
- [3] A. S. Bhalla, R. Guo, and R. Roy, *The perovskite structure - a review of its role in ceramic science and technology*, Mater. Res. Innov. **4**, 3 (2000).
- [4] E. Wainer, *High Titania Dielectrics*, Trans. Electrochem. Soc. **89**, 331 (1946).
- [5] M. E. Lines and A. M. Glass, *Principles and applications of ferroelectrics and related materials* (Oxford University Press, Oxford, Great Britain, 1977).
- [6] B. Jaffe, W. R. Cook, and H. Jaffe, *Piezoelectric ceramics* (Academic Press, Berkeley Square House, Berkeley Square, London, 1971).
- [7] R. von Helmolt, J. Wecker, B. Holzapfel, L. Schultz, and K. Samwer, *Giant negative magnetoresistance in perovskitelike  $La_{2/3}Ba_{1/3}MnO_x$  ferromagnetic films*, Phys. Rev. Lett. **71**, 2331 (1993).
- [8] Y. Moritomo, A. Asamitsu, H. Kuwahara, and Y. Tokura, *Giant magnetoresistance of manganese oxides with a layered perovskite structure*, Nature **380**, 141 (1996).
- [9] T. Okuda, K. Nakanishi, S. Miyasaka, and Y. Tokura, *Large thermoelectric response of metallic perovskites:  $Sr_{1-x}La_xTiO_3$  ( $0 < x < 0.1$ )*, Phys. Rev. B **63**, 113104 (2001).
- [10] J. F. Schooley, W. R. Hosler, E. Ambler, J. H. Becker, M. L. Cohen, and C. S. Koonce, *Dependence of the Superconducting Transition Temperature on Carrier Concentration in Semiconducting  $SrTiO_3$* , Phys. Rev. Lett. **14**, 305 (1965).

## Bibliography

---

- [11] D. Johnston, H. Prakash, W. Zachariasen, and R. Viswanathan, *High temperature superconductivity in the Li-Ti-O ternary system*, Mater. Res. Bull. **8**, 777 (1973).
- [12] K. Funke, *Solid State Ionics: from Michael Faraday to green energy—the European dimension*, Sci. Technol. Adv. Mater. **14**, 043502 (2013).
- [13] A. Wells, *Structural Inorganic Chemistry (fifth edition)* (Oxford University Press, Oxford, Great Britain, 1987).
- [14] V. M. Goldschmidt, *Die Gesetze der Krystallochemie*, Naturwissenschaften **14**, 477 (1926).
- [15] R. D. Shannon and IUCr, *Revised effective ionic radii and systematic studies of interatomic distances in halides and chalcogenides*, Acta Crystallogr. Sect. A **32**, 751 (1976).
- [16] L. A. Reznichenko, L. A. Shilkina, S. V. Titov, O. N. Razumovskaya, V. V. Titov, and S. I. Shevtsov, *Defect Structure of Alkaline-Earth, Cadmium, and Lead Titanates*, Inorg. Mater. **41**, 492 (2005).
- [17] A. M. Glazer, *The classification of tilted octahedra in perovskites*, Acta Crystallogr. Sect. B Struct. Crystallogr. Cryst. Chem. **28**, 3384 (1972).
- [18] A. M. Glazer, *Simple ways of determining perovskite structures*, Acta Crystallogr. Sect. A **31**, 756 (1975).
- [19] N. A. Benedek and C. J. Fennie, *Why Are There So Few Perovskite Ferroelectrics?*, J. Phys. Chem. C **117**, 13339 (2013).
- [20] S. B. Adler, *Chemical Expansivity of Electrochemical Ceramics*, J. Am. Ceram. Soc. **84**, 2117 (2001).
- [21] A. K. E. Andersson, S. M. Selbach, C. S. Knee, and T. Grande, *Chemical Expansion Due to Hydration of Proton-Conducting Perovskite Oxide Ceramics*, J. Am. Ceram. Soc. **97**, 2654 (2014).
- [22] F. G. Kinyanjui, S. T. Norberg, I. Ahmed, S. G. Eriksson, and S. Hull, *In-situ conductivity and hydration studies of proton conductors using neutron powder diffraction*, Solid State Ionics **225**, 312 (2012).
- [23] C. Hiraiwa, D. Han, A. Kuramitsu, A. Kuwabara, H. Takeuchi, M. Majima, and T. Uda, *Chemical Expansion and Change in Lattice Constant of Y-Doped BaZrO<sub>3</sub> by Hydration/Dehydration Reaction and Final Heat-Treating Temperature*, J. Am. Ceram. Soc. **96**, 879 (2013).

- 
- [24] C. Chatzichristodoulou, P. Norby, P. V. Hendriksen, and M. B. Mogensen, *Size of oxide vacancies in fluorite and perovskite structured oxides*, *J. Electroceramics* **34**, 100 (2014).
- [25] D. Marrocchelli, S. R. Bishop, H. L. Tuller, and B. Yildiz, *Understanding Chemical Expansion in Non-Stoichiometric Oxides: Ceria and Zirconia Case Studies*, *Adv. Funct. Mater.* **22**, 1958 (2012).
- [26] D. Marrocchelli, S. R. Bishop, H. L. Tuller, G. W. Watson, B. Yildiz, P. A. Madden, P. A. Madden, G. W. Watson, and E. D. Wachsman, *Charge localization increases chemical expansion in cerium-based oxides*, *Phys. Chem. Chem. Phys.* **14**, 12070 (2012).
- [27] S. R. Bishop, K. L. Duncan, and E. D. Wachsman, *Thermo-Chemical Expansion in Strontium-Doped Lanthanum Cobalt Iron Oxide*, *J. Am. Ceram. Soc.* **93**, 4115 (2010).
- [28] S. A. Centoni, B. Sadigh, G. H. Gilmer, T. J. Lenosky, T. Díaz de la Rubia, and C. B. Musgrave, *First-principles calculation of intrinsic defect formation volumes in silicon*, *Phys. Rev. B* **72**, 195206 (2005).
- [29] F. W. Poulsen, *Speculations on the existence of hydride ions in proton conducting oxides*, *Solid State Ionics* **145**, 387 (2001).
- [30] T. Norby, M. Widerøe, R. Glöckner, and Y. Larring, *Hydrogen in oxides*, *Dalt. Trans.* **0**, 3012 (2004).
- [31] R. M. Helps, N. H. Rees, and M. A. Hayward, *Sr<sub>3</sub>Co<sub>2</sub>O<sub>4.33</sub>H<sub>0.84</sub> : An Extended Transition Metal Oxide-Hydride*, *Inorg. Chem.* **49**, 11062 (2010).
- [32] Y.-D. Chuang, A. D. Gromko, D. S. Dessau, T. Kimura, Y. Tokura, C. J. Kiely, S. J. Blundell, I. M. Marshall, and F. L. Pratt, *Fermi Surface Nesting and Nanoscale Fluctuating Charge/Orbital Ordering in Colossal Magnetoresistive Oxides*, *Science* **292**, 1509 (2001).
- [33] Y. Kobayashi, O. J. Hernandez, T. Sakaguchi, T. Yajima, T. Roisnel, Y. Tsujimoto, M. Morita, Y. Noda, Y. Mogami, A. Kitada, M. Ohkura, S. Hosokawa, Z. Li, K. Hayashi, Y. Kusano, J. eun Kim, N. Tsuji, A. Fujiwara, Y. Matsushita, K. Yoshimura, K. Takegoshi, M. Inoue, M. Takano, and H. Kageyama, *An oxyhydride of BaTiO<sub>3</sub> exhibiting hydride exchange and electronic conductivity.*, *Nat. Mater.* **11**, 507 (2012).
- [34] T. Sakaguchi, Y. Kobayashi, T. Yajima, M. Ohkura, C. Tassel, F. Takeiri, S. Mitsuoka, H. Ohkubo, T. Yamamoto, J. eun Kim, N. Tsuji, A. Fujihara, Y.

## Bibliography

---

- Matsushita, J. Hester, M. Avdeev, K. Ohoyama, and H. Kageyama, *Oxyhydrides of (Ca,Sr,Ba)TiO<sub>3</sub> Perovskite Solid Solutions*, Inorg. Chem. **51**, 11371 (2012).
- [35] Y. Iwazaki, T. Suzuki, and S. Tsuneyuki, *Negatively charged hydrogen at oxygen-vacancy sites in BaTiO<sub>3</sub>: Density-functional calculation*, J. Appl. Phys. **108**, 1 (2010).
- [36] X. Liu, T. S. Bjorheim, and R. Haugsrud, *Formation and migration of hydride ions in BaTiO<sub>3-x</sub>H<sub>x</sub> oxyhydride*, J. Mater. Chem. A **5**, 1050 (2017).
- [37] G. Bouilly, T. Yajima, T. Terashima, W. Yoshimune, K. Nakano, C. Tassel, Y. Kususe, K. Fujita, K. Tanaka, T. Yamamoto, Y. Kobayashi, and H. Kageyama, *Electrical Properties of Epitaxial Thin Films of Oxyhydrides ATiO<sub>3-x</sub>H<sub>x</sub> (A = Ba and Sr)*, Chem. Mater. **27**, 6354 (2015).
- [38] L. Landau and S. Pekar, *Polaron effective mass*, Zh Eksp Teor Fiz **18**, 419 (1948).
- [39] J. T. Devreese, *Polarons*, Encycl. Appl. Phys. **14**, 383 (2000).
- [40] H. Fröhlich, *Electrons in lattice fields*, Adv. Phys. **3**, 325 (1954).
- [41] R. P. Feynman, *Slow Electrons in a Polar Crystal*, Phys. Rev. **97**, 660 (1955).
- [42] R. P. Feynman, R. W. Hellwarth, C. K. Iddings, and P. M. Platzman, *Mobility of Slow Electrons in a Polar Crystal*, Phys. Rev. **127**, 1004 (1962).
- [43] N. A. Deskins and M. Dupuis, *Electron transport via polaron hopping in bulk TiO<sub>2</sub>: A density functional theory characterization*, Phys. Rev. B **75**, 195212 (2007).
- [44] A. Janotti, J. B. Varley, P. Rinke, N. Umezawa, G. Kresse, and C. G. Van de Walle, *Hybrid functional studies of the oxygen vacancy in TiO<sub>2</sub>*, Phys. Rev. B **81**, 085212 (2010).
- [45] A. Janotti, C. Franchini, J. B. Varley, G. Kresse, and C. G. Van de Walle, *Dual behavior of excess electrons in rutile TiO<sub>2</sub>*, Phys. status solidi - Rapid Res. Lett. **7**, 199 (2013).
- [46] M. Setvin, C. Franchini, X. Hao, M. Schmid, A. Janotti, M. Kaltak, C. Van de Walle, G. Kresse, and U. Diebold, *A direct view at excess electrons in TiO<sub>2</sub> rutile and anatase*, Phys. Rev. Lett. **113**, 086402 (2014).
- [47] S. Yang, A. T. Brant, N. C. Giles, and L. E. Halliburton, *Intrinsic small polarons in rutile TiO<sub>2</sub>*, Phys. Rev. B **87**, 125201 (2013).

- 
- [48] V. M. Khomenko, K. Langer, H. Rager, and A. Fett, *Electronic absorption by  $Ti^{3+}$  ions and electron delocalization in synthetic blue rutile*, Phys. Chem. Miner. **25**, 338 (1998).
- [49] R. Scharfschwerdt, A. Mazur, O. F. Schirmer, H. Hesse, and S. Mendricks, *Oxygen vacancies in  $BaTiO_3$* , Phys. Rev. B **54**, 15284 (1996).
- [50] M. Schrader, D. Mienert, T.-S. Oh, H.-I. Yoo, and K. D. Becker, *An optical, EPR and electrical conductivity study of blue barium titanate,  $BaTiO_{3-\delta}$* , Solid State Sci. **10**, 768 (2008).
- [51] J. Maier, *Physical chemistry of ionic materials: ions and electrons in solids* (John Wiley & Sons, West Sussex, England, 2004).
- [52] S. Zhang and J. Northrup, *Chemical potential dependence of defect formation energies in GaAs: Application to Ga self-diffusion*, Phys. Rev. Lett. **67**, 2339 (1991).
- [53] C. Freysoldt, B. Grabowski, T. Hickel, J. Neugebauer, G. Kresse, A. Janotti, and C. G. Van de Walle, *First-principles calculations for point defects in solids*, Rev. Mod. Phys. **86**, 253 (2014).
- [54] S. Lany and A. Zunger, *Assessment of correction methods for the band-gap problem and for finite-size effects in supercell defect calculations: Case studies for ZnO and GaAs*, Phys. Rev. B **78**, 235104 (2008).
- [55] C. Freysoldt, J. Neugebauer, and C. G. Van de Walle, *Electrostatic interactions between charged defects in supercells*, Phys. status solidi **248**, 1067 (2011).
- [56] H.-P. Komsa, T. T. Rantala, and A. Pasquarello, *Finite-size supercell correction schemes for charged defect calculations*, Phys. Rev. B **86**, 045112 (2012).
- [57] *NIST Computational Chemistry Comparison and Benchmark Database NIST Standard Reference Database Number 101, Release 18, Editor: Russell D. Johnson III*, <http://cccbdb.nist.gov>.
- [58] *NIST JANAF thermochemical tables 1985, Editor: Malcolm W. Chase Jr*, <http://kinetics.nist.gov/janaf>.
- [59] T. S. Bjørheim, M. Arrigoni, D. Gryaznov, E. Kotomin, and J. Maier, *Thermodynamic properties of neutral and charged oxygen vacancies in  $BaZrO_3$  based on first principles phonon calculations.*, Phys. Chem. Chem. Phys. **17**, 20765 (2015).

## Bibliography

---

- [60] S. Grieshammer, T. Zacherle, and M. Martin, *Entropies of defect formation in ceria from first principles*, Phys. Chem. Chem. Phys. **15**, 15935 (2013).
- [61] P. Ágoston and K. Albe, *Formation entropies of intrinsic point defects in cubic  $In_2O_3$  from first-principles density functional theory calculations*, Phys. Chem. Chem. Phys. **11**, 3226 (2009).
- [62] H. B. Huntington, G. A. Shirn, and E. S. Wajda, *Calculation of the Entropies of Lattice Defects*, Phys. Rev. **99**, 1085 (1955).
- [63] A. Togo, L. Chaput, I. Tanaka, and G. Hug, *First-principles phonon calculations of thermal expansion in  $Ti_3SiC_2$ ,  $Ti_3AlC_2$ , and  $Ti_3GeC_2$* , Phys. Rev. B **81**, 174301 (2010).
- [64] A. Togo and I. Tanaka, *First principles phonon calculations in materials science*, Scr. Mater. **108**, 1 (2015).
- [65] H. B. Callen, *Thermodynamics* (Wiley & Sons, New York, N.Y., 1960 (p.213-219)), p. 213.
- [66] C. Kittel, *Introduction to Solid State Physics (eighth edition)* (Wiley & Sons, New York, N.Y., 2005 (p.73-75)).
- [67] A. Nowic and B. Berry, *Anelastic Relaxation in Crystalline Solids* (Academic Press, London, 1972).
- [68] G. A. Holzapfel, *Nonlinear Solid Mechanics: A Continuum Approach for Engineering* (Wiley, Chichester, New York, 2000 (chap. 2)).
- [69] L. Kantorovich, *Quantum Theory of the Solid State: An Introduction* (Springer Netherlands, Dordrecht, 2004).
- [70] E. Kaxiras, *Atomic and Electronic Structure of Solids* (Cambridge University Press, The Edinburgh Building, Cambridge, United Kingdom, 2003).
- [71] N. Ashcroft and N. Mermin, *Solid state physics* (Brooks/Cole Cengage Learning, Belmont, Ca, USA, 1976).
- [72] J. Thijssen, *Computational Physics* (Cambridge University Press, The Edinburgh Building, Cambridge, United Kingdom, 2007).
- [73] R. Martin, *Electronic Structure* (Cambridge University Press, The Edinburgh Building, Cambridge, United Kingdom, 2008).
- [74] A. D. Becke, *Perspective: Fifty years of density-functional theory in chemical physics*, J. Chem. Phys. **140**, 18A301 (2014).

- 
- [75] R. O. Jones, *Density functional theory: Its origins, rise to prominence, and future*, Rev. Mod. Phys. **87**, 897 (2015).
- [76] W. Kohn, *Nobel Lecture: Electronic structure of matter—wave functions and density functionals*, Rev. Mod. Phys. **71**, 1253 (1999).
- [77] J. P. Perdew and A. Zunger, *Self-interaction correction to density-functional approximations for many-electron systems*, Phys. Rev. B **23**, 5048 (1981).
- [78] L. H. Thomas, *The calculation of atomic fields*, Math. Proc. Cambridge Philos. Soc. **23**, 542 (1927).
- [79] E. Fermi, *Un metodo statistico per la determinazione di alcune proprieta dell'atome*, Rend. Accad. Naz. Lincei **65**, 602 (1927).
- [80] P. Dirac, *Note on exchange phenomena in the Thomas atom*, Math. Proc. Cambridge Philos. Soc. **26**, 376 (1930).
- [81] P. Hohenberg and W. Kohn, *Inhomogeneous Electron Gas*, Phys. Rev. **136**, B864 (1964).
- [82] W. Kohn and L. J. Sham, *Self-Consistent Equations Including Exchange and Correlation Effects*, Phys. Rev. **140**, A1133 (1965).
- [83] M. G. Medvedev, I. S. Bushmarinov, J. Sun, J. P. Perdew, and K. A. Lyssenko, *Density functional theory is straying from the path toward the exact functional*, Science **355**, 49 (2017).
- [84] L. Hedin and B. I. Lundqvist, *Explicit local exchange-correlation potentials*, J. Phys. C Solid State Phys. **4**, 2064 (1971).
- [85] J. P. Perdew and Y. Wang, *Accurate and simple analytic representation of the electron-gas correlation energy*, Phys. Rev. B **45**, 13244 (1992).
- [86] D. M. Ceperley and B. J. Alder, *Ground State of the Electron Gas by a Stochastic Method*, Phys. Rev. Lett. **45**, 566 (1980).
- [87] J. P. Perdew, K. Burke, and M. Ernzerhof, *Generalized Gradient Approximation Made Simple*, Phys. Rev. Lett. **77**, 3865 (1996).
- [88] K. Burke, *Perspective on density functional theory*, J. Chem. Physics **136**, 150901 (2012).
- [89] J. P. Perdew, M. Ernzerhof, and K. Burke, *Rationale for mixing exact exchange with density functional approximations*, J. Chem. Phys. **105**, 9982 (1996).

## Bibliography

---

- [90] J. Heyd, G. E. Scuseria, and M. Ernzerhof, *Hybrid functionals based on a screened Coulomb potential*, J. Chem. Phys. **118**, 8207 (2003).
- [91] J. Heyd, G. E. Scuseria, and M. Ernzerhof, *Erratum: "Hybrid functionals based on a screened Coulomb potential" [J. Chem. Phys. 118, 8207 (2003)]*, J. Chem. Phys. **124**, 219906 (2006).
- [92] V. I. Anisimov, J. Zaanen, and O. K. Andersen, *Band theory and Mott insulators: Hubbard  $U$  instead of Stoner  $I$* , Phys. Rev. B **44**, 943 (1991).
- [93] S. L. Dudarev, G. A. Botton, S. Y. Savrasov, C. J. Humphreys, and A. P. Sutton, *Electron-energy-loss spectra and the structural stability of nickel oxide: An LSDA+ $U$  study*, Phys. Rev. B **57**, 1505 (1998).
- [94] A. Janotti, D. Segev, and C. G. Van de Walle, *Effects of cation  $d$  states on the structural and electronic properties of III-nitride and II-oxide wide-band-gap semiconductors*, Phys. Rev. B **74**, 045202 (2006).
- [95] P. Erhart, K. Albe, and A. Klein, *First-principles study of intrinsic point defects in ZnO: Role of band structure, volume relaxation, and finite-size effects*, Phys. Rev. B **73**, 205203 (2006).
- [96] J. P. Perdew, R. G. Parr, M. Levy, and J. L. Balduz, *Density-Functional Theory for Fractional Particle Number: Derivative Discontinuities of the Energy*, Phys. Rev. Lett. **49**, 1691 (1982).
- [97] H. J. Monkhorst and J. D. Pack, *Special points for Brillouin-zone integrations*, Phys. Rev. B **13**, 5188 (1976).
- [98] W. E. Pickett, *Pseudopotential methods in condensed matter applications*, Comput. Phys. Reports **9**, 115 (1989).
- [99] D. Vanderbilt, *Soft self-consistent pseudopotentials in a generalized eigenvalue formalism*, Phys. Rev. B **41**, 7892 (1990).
- [100] P. E. Blöchl, *Generalized separable potentials for electronic-structure calculations*, Phys. Rev. B **41**, 5414 (1990).
- [101] P. E. Blöchl, *Projector augmented-wave method*, Phys. Rev. B **50**, 17953 (1994).
- [102] G. Kresse and D. Joubert, *From ultrasoft pseudopotentials to the projector augmented-wave method*, Phys. Rev. B **59**, 1758 (1999).

- 
- [103] A. Kiejna, G. Kresse, J. Rogal, A. De Sarkar, K. Reuter, and M. Scheffler, *Comparison of the full-potential and frozen-core approximation approaches to density-functional calculations of surfaces*, Phys. Rev. B **73**, 035404 (2006).
- [104] A. Ghysels, V. Van Speybroeck, E. Pauwels, S. Catak, B. R. Brooks, D. Van Neck, and M. Waroquier, *Comparative study of various normal mode analysis techniques based on partial Hessians*, J. Comput. Chem. **31**, 994 (2009).
- [105] H. Li and J. H. Jensen, *Partial Hessian vibrational analysis: the localization of the molecular vibrational energy and entropy*, Theor. Chem. Acc. **107**, 211 (2002).
- [106] A. Togo and I. Tanaka, *Evolution of crystal structures in metallic elements*, Phys. Rev. B **87**, 184104 (2013).
- [107] A. Togo, L. Chaput, and I. Tanaka, *Distributions of phonon lifetimes in Brillouin zones*, Phys. Rev. B **91**, 094306 (2015).
- [108] W. Zhong and D. Vanderbilt, *Effect of quantum fluctuations on structural phase transitions in SrTiO<sub>3</sub> and BaTiO<sub>3</sub>*, Phys. Rev. B **53**, 5047 (1996).



# Paper I

## **Size and shape of oxygen vacancies and protons in acceptor-doped barium zirconate**

Erik Jedvik, Anders Lindman, Magnús Þór Benediktsson and Göran Wahnström  
Solid State Ionics 275 (2015) 2-8



# Paper II

## **Vibrational characterization of electronic defects in oxyhydride barium titanate**

Erik Jedvik Granhed, Anders Lindman, Carin Österberg, Maths Karlsson and  
Göran Wahnström

To be Submitted